Published for SISSA by Springer

Received: November 18, 2022
Revised: December 17, 2022
Accepted: December 30, 2022
Published: January 18, 2023

The scalar singlet extension of the Standard Model: gravitational waves versus baryogenesis

John Ellis,[a,b,c] **Marek Lewicki,**[d] **Marco Merchand,**[d] **José Miguel No**[e,f] **and Mateusz Zych**[d]

[a] *Department of Physics, King's College London, Strand, London WC2R 2LS, U.K.*
[b] *Theoretical Physics Department, CERN, Geneva, Switzerland*
[c] *National Institute of Chemical Physics & Biophysics, Rävala 10, 10143 Tallinn, Estonia*
[d] *Faculty of Physics, University of Warsaw, ul. Pasteura 5, 02-093 Warsaw, Poland*
[e] *Instituto de Física Teórica, IFT-UAM/CSIC, Cantoblanco, 28049 Madrid, Spain*
[f] *Departamento de Física Teórica, Universidad Autónoma de Madrid, 28049 Madrid, Spain*

E-mail: John.Ellis@cern.ch, marek.lewicki@fuw.edu.pl, mmerchand@fuw.edu.pl, Josemiguel.no@uam.es, mateusz.zych@fuw.edu.pl

Abstract: We study the possible gravitational wave signal and the viability of baryogenesis arising from the electroweak phase transition in an extension of the Standard Model (SM) by a scalar singlet field without a $\mathbb{Z}_2$ symmetry. We first analyze the velocity of the expanding true-vacuum bubbles during the phase transition, confirming our previous finding in the unbroken $\mathbb{Z}_2$ symmetry scenario, where the bubble wall velocity can be computed from first principles only for weak transitions with strength parameters $\alpha \lesssim 0.05$, and the Chapman-Jouguet velocity defines the maximum velocity for which the wall is stopped by the friction from the plasma. We further provide an analytical approximation to the wall velocity in the general scalar singlet scenario without $\mathbb{Z}_2$ symmetry and test it against the results of a detailed calculation, finding good agreement. We show that in the singlet scenario with a spontaneously broken $\mathbb{Z}_2$ symmetry, the phase transition is always weak and we see no hope for baryogenesis. In contrast, in the case with explicit $\mathbb{Z}_2$ breaking there is a region of the parameter space producing a promising baryon yield in the presence of CP violating interactions via an effective operator involving the singlet scalar and the SM top quarks. Yet, we find that this region yields unobservable gravitational waves. Finally, we show that the promising region for baryogenesis in this model may be fully tested by direct searches for singlet-like scalars in di-boson final states at the HL-LHC, combined with present and future measurements of the electron electric dipole moment.

Keywords: Baryo-and Leptogenesis, Phase Transitions in the Early Universe

ArXiv ePrint: 2210.16305

https://doi.org/10.1007/JHEP01(2023)093

Contents

JHEP01(2023)093

1 Introduction

The lack of an explanation within the Standard Model (SM) for the observed baryon asymmetry of the Universe is one of the key motivations for studying scenarios for physics beyond the SM (BSM). One attractive scenario is that baryogenesis be associated with the electroweak scale, potentially maximizing its testability in laboratory experiments [1–4]. However, electroweak baryogenesis (EWBG) would require a first-order phase transition (FOPT) at the electroweak scale, which does not occur in the SM [5]. If it were to occur in some BSM scenario, collisions between bubbles of the low-energy vacuum and the ensuing turbulence and sound waves in the primordial plasma might have generated a stochastic cosmological background of gravitational waves (GWs) large enough to be detectable in future experiments such as LISA [6, 7] or AEDGE [8, 9].

This possibility has stimulated increased interest in BSM scenarios involving a FOPT [10–62]. Scenarios for electroweak baryogenesis exploit the fact that electroweak

sphalerons are active and postulate a CP-violating force that generates a matter-antimatter asymmetry in chemical potentials. At the end of the transition when the sphaleron rate is suppressed, this asymmetry freezes out into the net baryon number observed today.

One of the simplest scenarios capable of producing a FOPT invokes a gauge singlet scalar in addition to the SM [63–65]. In spite of its minimality, this scenario offers a vast array of possibilities for phenomenological studies, including collider searches, sensitivities and constraints [64, 66–69], dark scalar cosmological constraints [70, 71], dark matter [72–75], gravitational wave production [76] and baryogenesis [77, 78]. In particular, the complementarity between collider searches and GW experiments for probing the parameter space of the model has been studied extensively [28, 79–82].

Implementing EWBG within this scalar singlet extension of the SM requires the introduction of extra sources of CP violation. This is usually achieved by adding higher-dimension operators to the Lagrangian in order to keep the particle content minimal. However, these operators are subject to tight constraints from experimental upper bounds on electric dipole moments (EDMs), unless they are made to vanish at zero temperature. To the best of our knowledge, the EWBG computation has not been performed in the most generic scenario with a non-vanishing vev for the scalar singlet, and computations of the baryon asymmetry have been focused on the case in which the singlet has a vanishing vev. On the other hand, studies of the potential synergy between colliders and GW experiments for probing the region of parameter space compatible with EWBG have mainly focused on the scenario with non-vanishing singlet vev [79–81], while remaining agnostic about the source(s) of CP violation.[1]

The aim of the present paper is to plug this gap by investigating the viability of EWBG in the scalar singlet extension of the SM using the most general parametrization of the scalar potential and assuming a non-vanishing vev for the singlet. As CP-violating source we include a dimension-five operator coupling the singlet field with the Higgs-top Yukawa interaction. The final baryon yield is computed via the WKB formalism [83–85].[2] We find that, due to the presence of the higher dimensional operator involving the singlet and the SM top quarks (as needed here for baryogenesis), future LHC searches for singlet-like scalars in di-boson final states will be able to probe this baryogenesis scenario even in the limit of very small singlet-Higgs mixing.

We provide at the same time updated predictions for the GW signals taking into account a full computation of the properties of the bubble wall using the fluid equations of the new formalism of [92, 93]. Thus we extend our previous work [94] on the properties of bubble walls in SM-like thermal plasmas, showing that the same qualitative conclusions apply for this model.

The rest of the paper is outlined as follows: in section 2 we introduce the model focusing on the effective potential. Section 3 dynamics of the phase transition. In section 4 we focus on the case of spontaneous $\mathbb{Z}_2$ symmetry breaking. We show that the transitions

[1] See, however, [68] for an exception.

[2] An alternative method is given by the vev-insertion approximation (VIA) [86, 87] which generically yields $\mathcal{O}(10)$ larger values for the baryon asymmetry although it was recently claimed to be not fully consistent [88, 89]. See refs. [90, 91] for comparative studies of these formalisms.

JHEP01(2023)093

in that case are always too weak to give hope for baryogenesis, and move on to the case of explicit $\mathbb{Z}_2$ symmetry breaking in the remainder of the paper. Section 5 discusses the computation of the bubble wall properties as well as the analytical approximation of the bubble wall velocity and its accuracy. Using these results in section 6 we discuss the GW signals the model can produce. In section 7 we discuss our scenario for baryogenesis, first setting out the phenomenological constraints on the CP-violating model and then discussing the possible magnitude of the cosmological baryon asymmetry. We highlight the part of parameter space that yields results consistent with cosmology, and discuss the possible LHC and EDM probes of this region. Section 8 summarizes our conclusions. The issues of vacuum stability and perturbativity are discussed in an appendix.

2 The effective potential of the singlet scalar extension of the SM

2.1 Tree-level potential

The model we consider in this paper has been studied previously in refs. [33, 64, 81], and the complementarity between its signatures in GW and collider experiments was studied in [28]. The tree-level scalar potential of the model is

$$V_0(H,s) = -\mu_h^2 H^\dagger H + \lambda_h (H^\dagger H)^2 - \frac{1}{2}\mu_s^2 s^2 + \frac{1}{4}\lambda_s s^4 + \frac{1}{2}\lambda_{hs} H^\dagger H s^2 + \mu_{hs} H^\dagger H s - \frac{1}{3}\mu_3 s^3, \quad (2.1)$$

where $H = (G^+, \frac{h+iG^0}{\sqrt{2}})^{\mathrm{T}}$ is the Higgs doublet with the SM vacuum expectation value (vev) $v = 246.2\,\mathrm{GeV}$, while s is the additional real scalar singlet. Eq. (2.1) is the most general formulation of the model, in which the $\mathbb{Z}_2$ symmetry of the potential corresponding to changing the sign of s is not assumed. In a unitary gauge the potential (2.1) can be written as

$$V_0(h,s) = -\frac{1}{2}\mu_h^2 h^2 + \frac{1}{4}\lambda_h h^4 - \frac{1}{2}\mu_s^2 s^2 + \frac{1}{4}\lambda_{hs} h^2 s^2 + \frac{1}{4}\lambda_s s^4 + \frac{1}{2}\mu_{hs} h^2 s - \frac{1}{3}\mu_3 s^3. \quad (2.2)$$

The electroweak symmetry-breaking (EWSB) vacuum is located at the field values $(h,s) = (v,u)$, where

$$\begin{aligned} \frac{\partial V_0}{\partial h}\Big|_{(v,u)} &= -\mu_h^2 v + \lambda_h v^3 + \frac{1}{2}\lambda_{hs} v u^2 + \mu_{hs} v u = 0\,, \\ \frac{\partial V_0}{\partial s}\Big|_{(v,u)} &= -\mu_s^2 u + \lambda_s u^3 + \frac{1}{2}\lambda_{hs} v^2 u + \frac{1}{2}\mu_{hs} v^2 - \mu_3 u^2 = 0\,, \end{aligned} \quad (2.3)$$

which lead to the following conditions

$$\begin{aligned} \mu_h^2 &= \lambda_h v^2 + \frac{1}{2}\lambda_{hs} u^2 + \mu_{hs} u\,, \\ \mu_s^2 &= \lambda_s u^2 + \frac{1}{2}\lambda_{hs} v^2 + \frac{1}{2}\mu_{hs}\frac{v^2}{u} - \mu_3 u\,. \end{aligned} \quad (2.4)$$

JHEP01(2023)093

The elements of the scalar mass matrix M are

$$\begin{aligned} M_{hh}^2 &= \frac{\partial^2 V_0}{\partial h^2}\Big|_{(v,u)} = -\mu_h^2 + 3\lambda_h v^2 + \frac{1}{2}\lambda_{hs}u^2 + \mu_{hs}u = \\ &= 2\lambda_h v^2\,, \\ M_{ss}^2 &= \frac{\partial^2 V_0}{\partial s^2}\Big|_{(v,u)} = -\mu_s^2 + 3\lambda_s u^2 + \frac{1}{2}\lambda_{hs}v^2 - 2\mu_3 u = \\ &= 2\lambda_s u^2 - \mu_3 u - \frac{1}{2u}\mu_{hs}v^2\,, \\ M_{hs}^2 &= \frac{\partial^2 V_0}{\partial h \partial s}\Big|_{(v,u)} = \lambda_{hs}vu + \mu_{hs}v\,. \end{aligned} \tag{2.5}$$

In order to obtain the physical scalar masses, one diagonalizes the mass matrix and introduces mass eigenstates φ_1, φ_2 given by

$$\begin{pmatrix}\varphi_1\\ \varphi_2\end{pmatrix} = \begin{pmatrix}\cos\theta & -\sin\theta\\ \sin\theta & \cos\theta\end{pmatrix}\begin{pmatrix}h\\ s\end{pmatrix}\,, \tag{2.6}$$

which satisfy

$$\begin{aligned} \begin{pmatrix}\varphi_1,\varphi_2\end{pmatrix}\begin{pmatrix}m_h^2 & 0\\ 0 & m_s^2\end{pmatrix}\begin{pmatrix}\varphi_1\\ \varphi_2\end{pmatrix} &= \begin{pmatrix}h,s\end{pmatrix}\begin{pmatrix}M_{hh}^2 & M_{hs}^2\\ M_{sh}^2 & M_{ss}^2\end{pmatrix}\begin{pmatrix}h\\ s\end{pmatrix} \\ &= \begin{pmatrix}\varphi_1,\varphi_2\end{pmatrix}\begin{pmatrix}\cos\theta & -\sin\theta\\ \sin\theta & \cos\theta\end{pmatrix}\begin{pmatrix}M_{hh}^2 & M_{hs}^2\\ M_{sh}^2 & M_{ss}^2\end{pmatrix}\begin{pmatrix}\cos\theta & \sin\theta\\ -\sin\theta & \cos\theta\end{pmatrix}\begin{pmatrix}\varphi_1\\ \varphi_2\end{pmatrix}. \end{aligned} \tag{2.7}$$

Comparing corresponding elements in these matrix equations, one obtains

$$\begin{aligned} m_h^2 &= M_{hh}^2\cos^2\theta + M_{ss}^2\sin^2\theta - M_{hs}^2\sin 2\theta\,, \\ m_s^2 &= M_{hh}^2\sin^2\theta + M_{ss}^2\cos^2\theta + M_{hs}^2\sin 2\theta\,, \\ 0 &= -\frac{1}{2}(M_{ss}^2 - M_{hh}^2)\sin 2\theta + M_{hs}^2\cos 2\theta\,. \end{aligned} \tag{2.8}$$

Inverting the system, we find

$$\begin{aligned} M_{hh}^2 &= m_h^2\cos^2\theta + m_s^2\sin^2\theta\,, \\ M_{ss}^2 &= m_h^2\sin^2\theta + m_s^2\cos^2\theta\,, \\ M_{hs}^2 &= -m_h^2\sin\theta\cos\theta + m_s^2\sin\theta\cos\theta\,. \end{aligned} \tag{2.9}$$

After simplifications and using (2.5), we find the following conditions:

$$\begin{aligned} \lambda_h &= \frac{1}{2v^2}(m_h^2\cos^2\theta + m_s^2\sin^2\theta)\,, \\ \lambda_s &= \frac{1}{2u^2}\left(m_h^2\sin^2\theta + m_s^2\cos^2\theta + \mu_3 u + \frac{1}{2}\mu_{hs}\frac{v^2}{u}\right)\,, \\ \lambda_{hs} &= \frac{1}{vu}((m_s^2 - m_h^2)\sin\theta\cos\theta - \mu_{hs}v)\,. \end{aligned} \tag{2.10}$$

Positivity imposes the following requirement in addition to $\lambda_h, \lambda_s > 0$:

$$\lambda_{hs} > -2\sqrt{\lambda_h\lambda_s}, \quad \text{if} \quad \lambda_{hs} < 0\,. \tag{2.11}$$

JHEP01(2023)093

In our numerical study of the parameter space we impose perturbativity of the quartic couplings by requiring they satisfy the conditions

$$\lambda_h, \lambda_s, |\lambda_{hs}| \leq 4\pi \,. \tag{2.12}$$

2.2 One-loop effective potential

The full one-loop effective potential at finite temperature can be represented in general as

$$V_{\rm eff}(h, s, T) = V_0(h, s) + V_{\rm CW}(h, s) + V_{\rm T}(h, s, T) \,, \tag{2.13}$$

where V_0 is the tree-level potential, $V_{\rm CW}$ denotes the one-loop corrections known as the Coleman-Weinberg potential [95] and V_T represents the finite-temperature contribution. Using the cutoff regularization and on-shell renormalization scheme, the Coleman-Weinberg part is given by

$$V_{\rm CW}(h, s) = \sum_i (-1)^{F_i} \frac{d_i}{64\pi^2} \left[m_i^4(h, s) \left(\log \frac{m_i^2(h, s)}{m_{0i}^2} - \frac{3}{2} \right) + 2 m_i^2(h, s) m_{0i}^2 \right] , \tag{2.14}$$

where the index i runs over all particles contributing to the potential with $F_i = 0$ (1) for bosons (fermions), d_i is the number of degrees of freedom of the particle species, $m_i(h, s)$ is the field-dependent mass of particle i and m_{0i} its value in the EW vacuum of the SM. The field-dependent masses are given in the SM by

$$m_W^2 = \frac{g^2}{4} h^2, \quad m_Z^2 = \frac{g^2 + g'^2}{4} h^2, \quad m_t^2 = \frac{y_t^2}{2} h^2 \,. \tag{2.15}$$

The thermally-corrected masses of the scalars are the eigenvalues of the thermally-corrected Hessian matrix

$$M^2 \to M^2 + \begin{pmatrix} \Pi_h(T) & 0 \\ 0 & \Pi_s(T) \end{pmatrix} , \tag{2.16}$$

while for the longitudinal polarization states of vector bosons

$$m_W^2 \to m_W^2 + \Pi_W(T) \tag{2.17}$$

and

$$M_{Z/\gamma}^2 = \begin{pmatrix} \frac{1}{4} g^2 h^2 + \frac{11}{6} g^2 T^2 & -\frac{1}{4} g g' h^2 \\ -\frac{1}{4} g g' h^2 & \frac{1}{4} g'^2 h^2 + \frac{11}{6} g'^2 T^2 \end{pmatrix} . \tag{2.18}$$

The thermal masses in this model are found to be [96]

$$\Pi_h = \left(\frac{3g^2}{16} + \frac{g'^2}{16} + \frac{\lambda}{2} + \frac{y_t^2}{4} + \frac{\lambda_{hs}}{24} \right) T^2 \,, \tag{2.19}$$

$$\Pi_s = \left(\frac{\lambda_{hs}}{6} + \frac{\lambda_s}{4} \right) T^2 \,, \tag{2.20}$$

$$\Pi_W = \frac{11}{6} g^2 T^2 \,. \tag{2.21}$$

JHEP01(2023)093

These results are obtained by daisy resummation, which yields the following full finite-temperature expression:

$$V_T(\phi, T) = \frac{T^4}{2\pi^2} \sum_i d_i J_\mp \left(\frac{m_i(\phi)}{T} \right) , \tag{2.22}$$

where the $J_\mp$ functions are defined as

$$J_\mp(x) = \pm \int_0^\infty dy y^2 \log \left(1 \mp e^{-\sqrt{y^2+x^2}} \right) , \tag{2.23}$$

the upper (lower) sign is for bosons (fermions) and m_i refers to masses including the thermal corrections discussed above. The thermodynamic predictions using the effective potential at 1-loop have been considerably improved by 2-loop computations as well as non-perturbative dimensional reductions, see e.g., refs. [97–100]. We leave a diligent study of the sort for future work.

3 Phase transition dynamics: nucleation and percolation

The methods for computing the thermodynamic properties of a thermal FOPT in perturbative models are well established. One begins with the critical temperature T_c, defined to be the temperature at which multiple minima of the thermal effective potential become degenerate. One needs then to find the time of nucleation at which the probability of a true vacuum bubble forming within a horizon radius becomes significant, i.e.,

$$N(T_n) = \int_{T_n}^{T_c} \frac{dT}{T} \frac{\Gamma(T)}{H(T)^4} = 1 , \tag{3.1}$$

where

$$\Gamma(T) = \left(\frac{S_3}{2\pi T} \right)^{3/2} T^4 e^{-S_3/T} , \tag{3.2}$$

is the nucleation probability per unit time and volume, S_3 denotes the Euclidean action corresponding to the bounce solution and $H(T)$ is the Hubble expansion rate.

While computing the bounce for a model with a single scalar field is made relatively easy by use of a shooting algorithm, the task becomes significantly more onerous as the number of scalars increases. Moreover, one generally wishes to survey the full parameter space of the theory, compounding the problem. In this paper we use the publicly available code `cosmoTransitions` [101], which in principle can deal with an arbitrary number of scalars.

To leading-order accuracy and for temperatures close to the electroweak scale, the nucleation temperature can be obtained from the requirement

$$\frac{S_3}{T_n} \approx 140 , \tag{3.3}$$

which provides a good approximation for sufficiently weak transitions. This condition is already embedded in the public version of the `cosmoTransitions` code, and we use this version for a preliminary survey of the parameter space in which a FOPT occurs. However,

JHEP01(2023)093

when the transition becomes too strong, the formula presented above is only indicative and a more careful treatment is necessary in order to evaluate if nucleation actually occurs.

To assess if nucleation is possible we look for the solution to

$$\Gamma(T_n) = H_{\rm total}(T_n)^4\,, \tag{3.4}$$

with the highest temperature, and we use the total Hubble rate including the vacuum contribution, namely

$$H^2_{\rm total}(T) = \frac{g_*(T)\pi^2 T^4}{90 M^2_{\rm Pl}} + \frac{\Delta V(T)}{3M^2_{\rm Pl}}, \tag{3.5}$$

where g_* is the number of relativistic degrees of freedom [102] and $M_{\rm Pl} = 2.4 \times 10^{18}\,\text{GeV}$ is the reduced Planck mass.

In addition to determining when nucleation is possible, an essential question is whether the transition completes [103]. This can be answered by computing the temperature at which the probability of a point remaining in the false vacuum drops below 0.71 and then verifying that the false vacuum volume is indeed shrinking at that temperature, i.e.

$$I(T) = \frac{4\pi}{3}\int_T^{T_c} \frac{dT'}{H(T')}\Gamma(T')\frac{r(T,T')^3}{T'^4} = 0.34, \quad T\frac{dI(T)}{dT} < -3\,, \tag{3.6}$$

where

$$r(t,t') = v_w \int_{t'}^{t} \frac{d\tilde{t}}{a(\tilde{t})} \tag{3.7}$$

is the comoving radius of the bubble. The temperature at which the above two conditions are satisfied is referred to as the percolation temperature T_p.

To illustrate the importance of a careful nucleation assessment we show in figure 1 the nucleation rate and the Hubble parameter evaluated both with only radiation and with the full energy density including also the vacuum energy-difference term as functions of temperature for two benchmark points in the parameter space:

$$\begin{aligned}
&\text{P1}: \quad m_s = 168\,\text{GeV}, \quad \theta = 0.23, \quad u = -148\,\text{GeV}, \quad \mu_{hs} = 137\,\text{GeV}, \quad \mu_3 = -577\,\text{GeV}\,,\\
&\text{P2}: \quad m_s = 133\,\text{GeV}, \quad \theta = -0.02, \quad u = 129\,\text{GeV}, \quad \mu_{hs} = -137\,\text{GeV}, \quad \mu_3 = 566\,\text{GeV}\,.
\end{aligned}$$

For P1 the vacuum contribution is dominant and prevents nucleation from occurring. In contrast, for P2 the vacuum contribution is subdominant and we have checked that bubbles not only nucleate but also satisfy the condition for successful percolation.

4 Case of spontaneous $\mathbb{Z}_2$ symmetry breaking

As previously mentioned, the model we are studying can be described by five free parameters: m_s, θ, u, μ_{hs} and μ_3, which are the scalar singlet mass, the mixing angle with the SM Higgs boson, the singlet vacuum expectation value (vev) and the two $\mathbb{Z}_2$-breaking trilinear couplings, respectively. Before presenting the full results of our scans, we consider the pattern of the phase transitions in simplified scenarios. We start with the simplest scenario in which the potential is symmetric under a parity transformation of the fields. This case

JHEP01(2023)093

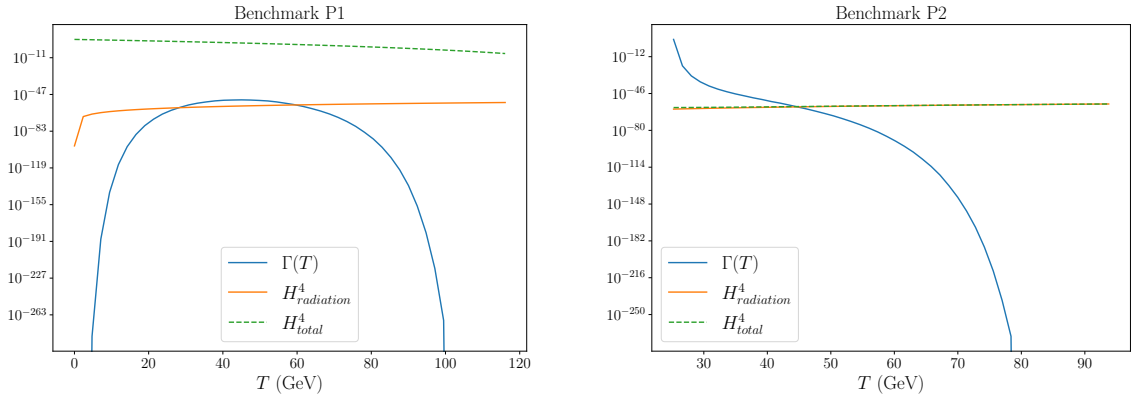

Figure 1. Rates as functions of temperature for the two benchmarks introduced in the text. Blue curves show the finite-temperature nucleation rates, orange lines the Hubble rates including only the radiation component and green dashed lines show the total Hubble rates with the vacuum contribution included.

corresponds to switching off the trilinear couplings, i.e., setting $\mu_{hs} = \mu_3 = 0$. The formulae for the quartic couplings now take the form

$$\begin{aligned} \lambda_h &= \frac{1}{2v^2}(m_h^2 \cos^2\theta + m_s^2 \sin^2\theta)\,, \\ \lambda_s &= \frac{1}{2u^2}(m_h^2 \sin^2\theta + m_s^2 \cos^2\theta)\,, \\ \lambda_{hs} &= \frac{1}{vu}((m_s^2 - m_h^2)\sin\theta\cos\theta)\,. \end{aligned} \tag{4.1}$$

It is important to remark that the parametrization adopted above renders it impossible to recover the scenario in which the singlet acquires no vev at zero temperature, usually referred to as xSM, as the limit $u \to 0$ is ill-defined mathematically. In the xSM model, studies have shown [94] that strong FOPTs are positively correlated with positive values of λ_{hs}. One might be tempted to infer that a similar trait also appears in the model under study, with the caveat that λ_s and λ_{hs} are no longer independent of each other as in the xSM case.

The model with a $\mathbb{Z}_2$-symmetric potential was already studied in [104]. The authors derived analytical expressions in the leading-order high-temperature expansion augmented with a trilinear term and neglecting the rest of the Coleman-Weinberg effective potential, for relevant quantities at the critical temperature and showed that the single parameter controlling these quantities is given by

$$\tilde{\lambda}_h = \lambda_h - \frac{\lambda_{hs}^2}{4\lambda_s}\,. \tag{4.2}$$

Here we calculate the parameters of the transition in this model using the full effective potential. Figure 2 compares our results with those obtained in the leading order high-temperature expansion and without the Coleman-Weinberg contribution, which match the analytical approximation discussed in [104]. In general, a correlation with the effective

JHEP01(2023)093

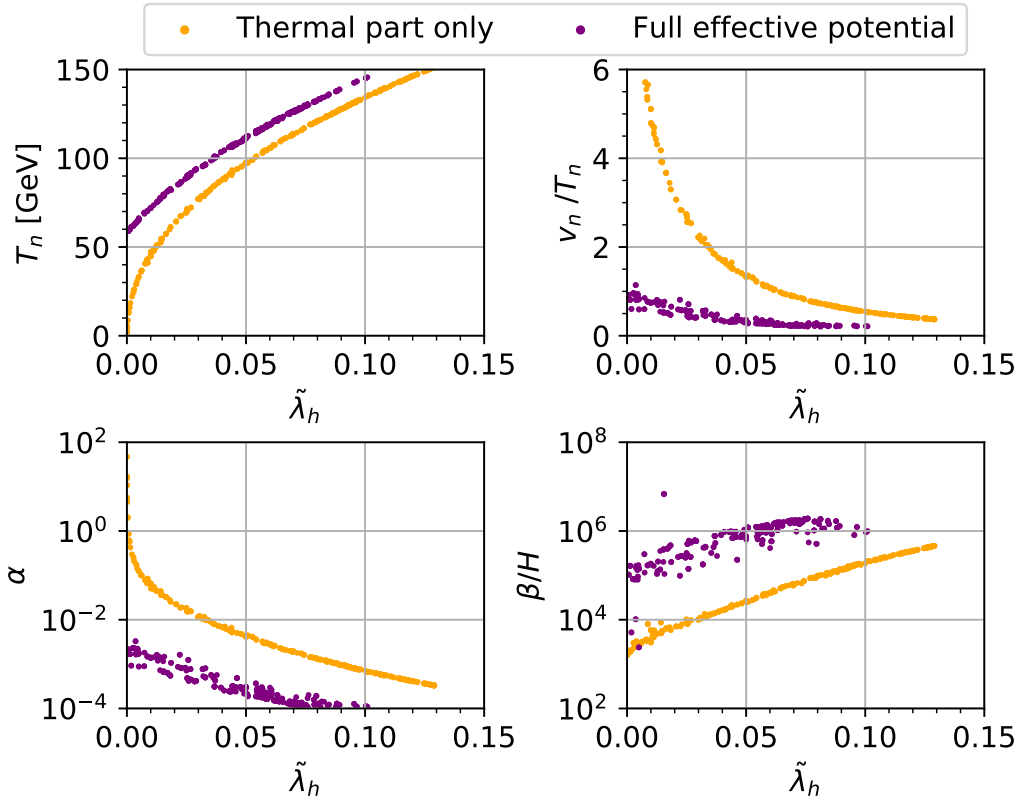

Figure 2. The phase transition parameters T_n, $\frac{v_n}{T_n}$, α and $\frac{\beta}{H}$ as functions of the effective coupling $\tilde{\lambda}_h$ for the thermally-corrected and full forms of the effective potential.

coupling $\tilde{\lambda}_h$ is still visible, but transitions using the full potential are significantly weaker. As $\tilde{\lambda}_h$ approaches λ_h, transitions become second-order and the trilinear coefficient E defined in [104] acquires its SM value. However, in the limit of stronger transitions tunnelling becomes singlet-driven, so the impact of the singlet becomes important, leading to vanishing E. Hence, for the strongest transitions possible in this model, the existence of the barrier is ensured at the tree level. In summary, we conclude that the $\mathbb{Z}_2$-symmetric version of the theory predicts only very weak transitions and cannot provide any significant observational predictions for GWs or baryogenesis. Therefore, we do not discuss this scenario further in the subsequent sections of this paper.[3]

5 Properties of the bubble wall

Estimating the properties of the bubble wall of a FOPT entails an involved computation of out-of-equilibrium perturbations in the plasma.[4] In addition, the form of the equations that should be used to obtain these estimates as well as the assumptions underlying them are not

[3]All our calculations were performed using the on-shell renormalization scheme, but we have verified that the results obtained using the MS-bar renormalization scheme are almost identical.

[4]The wall velocity has also been computed in strongly coupled theories via the holographic principle, see refs. [105, 106].

JHEP01(2023)093

agreed upon within the particle physics community. The most common presumptions are (i) that the bubble wall and the plasma particles interact in local thermal equilibrium [47, 107–110] or alternatively, (ii) that only the heaviest particles are taken out of thermal equilibrium by their interaction with the advancing wall but the rest of the particles in the plasma are treated as a background fluid in thermal equilibrium [111–114], henceforth called the *semiclassical fluid approximation*. In this paper we advocate the latter possibility and use the modified fluid equations of refs. [92, 93]. For alternative developments regarding assumption (ii) see [115–117].

The dynamics of the wall in the fluid approximation were first estimated in the pioneering papers [118, 119] for the SM electroweak theory with a light Higgs boson mass. Subsequently, the discovery of the Higgs boson prompted the adoption of this approximation in phenomenological models with a strong FOPT and not a crossover. The preferred model for study has been the scalar gauge singlet extension, either with a $\mathbb{Z}_2$-symmetric potential and no vev at zero temperature, see [93, 115, 120] or without the $\mathbb{Z}_2$ symmetry and non-vanishing vev at zero temperature [121]. Additionally, the SM effective field theory (SMEFT) with dimension-6 operator and a low cutoff was investigated in [122, 123].

We studied in [94] the generic implications that the *new formalism* (as dubbed in [117]) of [92, 93] has for the bubble wall properties in the $\mathbb{Z}_2$-symmetric singlet model with vanishing vev at zero temperature and in the SMEFT. One of the central results in [94] was that one can obtain a good numerical approximation for the wall speed using thermal equilibrium as a starting assumption. The following analytic formula was derived:

$$v_{\text{approx}} = \begin{cases} \sqrt{\frac{\Delta V}{\alpha \rho_r}} & \text{for} \quad \sqrt{\frac{\Delta V}{\alpha \rho_r}} < v_J(\alpha), \\ 1 & \text{for} \quad \sqrt{\frac{\Delta V}{\alpha \rho_r}} \geq v_J(\alpha)\,, \end{cases} \tag{5.1}$$

in which ΔV is the potential difference between the false and true vacua evaluated at the nucleation temperature, $\alpha \rho_r$ denotes the latent heat released and

$$v_J = \frac{1}{\sqrt{3}} \frac{1 + \sqrt{3\alpha^2 + 2\alpha}}{1 + \alpha}\,, \tag{5.2}$$

is the Chapman-Jouguet velocity [124–126]. The analytic approach was compared in [94] to the full computation for the two aforementioned BSM scenarios. The predictions of the two calculations were shown to agree well. This result is linked to the fact that the deviations from equilibrium are small and one can neglect temperature variations in the derivation of the analytic formula. This has been verified in [115], in which it was found that deviations from equilibrium are subdominant and that for sufficiently weak transitions a hydrodynamic treatment of the plasma shows that the bubble wall can reach a steady state.

In this paper we carry this analysis over to study the scalar singlet without $\mathbb{Z}_2$ symmetry and non-vanishing zero temperature vev. To the best of our knowledge, the computation of the bubble wall properties in this scenario has only been studied in ref. [121] using, however, the fluid equations laid out in [118, 119] that yield singularities for values of the wall velocity close to the speed of sound in the plasma. The computations in our work avoid this problem, and so represent a significantly improved assessment of the status of the model as a viable framework for electroweak baryogenesis.

JHEP01(2023)093

With regards to the algorithm used in [94], the scenario studied here requires only a minor modification. Clearly, the friction on the bubble wall in both the $\mathbb{Z}_2$-symmetric and non-symmetric cases is the same. Thus we follow the procedure of considering only the dominant contributions to the friction due to the electroweak gauge bosons and the top quark. The other particles, including the Higgs boson and singlet field, are treated as a background perturbations with zero chemical potential.

The necessary amendment for this scenario is due to the different form of scalar potential. In particular, the vacuum structure and the larger number of free parameters produce different features in the phase transition. For most values of the free parameters, the pattern of the transition starts from a high-temperature phase with zero Higgs vev and non-zero singlet vev (either positive or negative), and then tunnels towards the global minimum of the theory. As the field profiles should interpolate between the false and true vacua, we replace eqs. (4.14) and (4.15) in ref. [94] by the modified Ansatz

$$h(z) = \frac{h_0}{2}\left[\tanh\left(\frac{z}{L_h}\right) + 1\right], \tag{5.3}$$

$$s(z) = \frac{s_l - s_h}{2}\tanh\left(\frac{z}{L_s} - \delta_s\right) + \frac{s_h + s_l}{2}, \tag{5.4}$$

where h_0 is the Higgs vev at the true minimum and s_h and s_l represent the high-temperature (metastable) and low-temperature (stable) vevs of the singlet. The rest of the algorithm used in ref. [94] remains unchanged.

Results from the computation of the bubble wall velocity for a random scan of the parameter space are shown in figure 3, where the wall velocity is plotted against the strength of the transition and the coloured side-bar indicates the bubble wall width. The dash-dot-dotted orange line is the speed of sound in the plasma, $c_s = 1/\sqrt{3}$, below which the explosive growth of the bubble wall is a deflagration. The dashed orange line shows the Chapman-Jouguet velocity at a given value of α, while the magenta crosses are the value of the wall velocity obtained using the analytical approximation. In the region between the Chapman-Jouguet velocity and the speed of sound the explosive advancement of the bubble is a hybrid, i.e., it is composed of a shock discontinuity in front of the wall and a rarefaction wave behind it.

As shown in the figure, we cannot find steady-state solutions for points above the Chapman-Jouguet velocity. In those cases we expect the wall to reach highly relativistic velocities $v_w \approx 1$ and the expansion to proceed as a detonation. For some points of the random scan the analytic formula (corresponding to the magenta crosses) predicts $v_w = 1$ whereas in fact a steady-state solution can be obtained.

In order to quantify the applicability of the analytic approximation, we computed the sample mean percentage error between the analytic formula and the full computation:

$$\bar{v} \equiv \frac{1}{N}\sum_i^N \frac{|v_w - v_{\text{approx}}|}{v_w} \times 100 \approx 7.1\%, \tag{5.5}$$

which shows that the approximation provides a remarkably good estimate. The relative error for each parameter space point is shown in figure 4. The expansion profiles for

JHEP01(2023)093

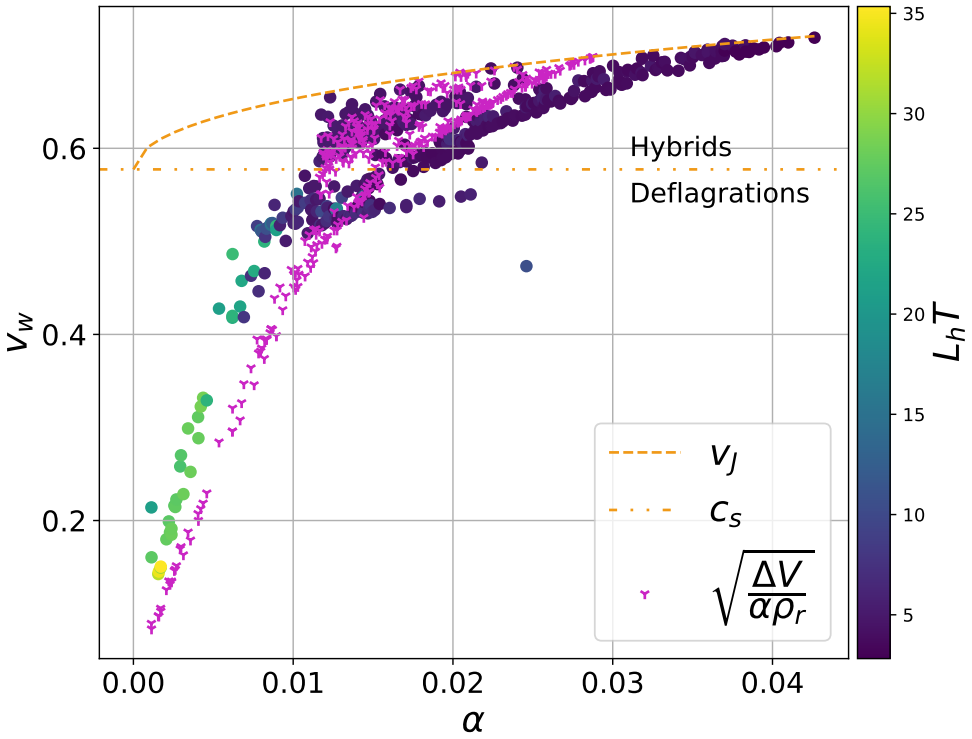

Figure 3. Predictions for the bubble wall velocity as a function of the strength α of the phase transition. The coloured side-bar gives the value of the Higgs profile thickness normalized to the nucleation temperature. The magenta crosses represent the values of the analytic approximation. The orange dashed and dash-dot-dotted lines represent the Chapman-Jouguet velocity and the speed of sound in the plasma, respectively.

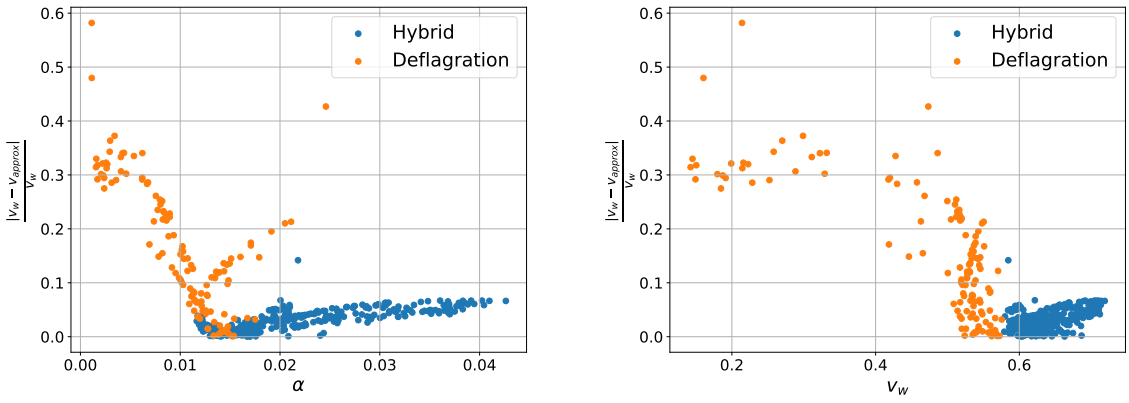

Figure 4. Relative errors in the wall velocity between the analytic approximation and the full calculation for deflagration points (orange) and hybrids (blue).

JHEP01(2023)093

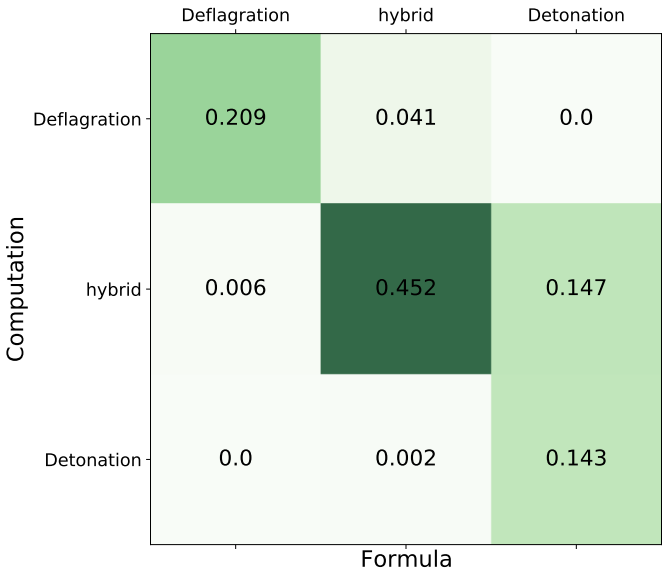

Figure 5. The confusion matrix for multi-class classification of the hydrodynamic expansion based on the computation of the wall velocity [127]. The rows (columns) denote the fraction of points that fall within each class as obtained from a full numerical computation (analytic formula).

deflagrations (hybrids) are shown as orange (blue). We find that the relative error is less than about ten percent for hybrid points, whereas deflagrations exhibit stronger deviations.

In order to assess further the utility of the analytic formula for classifying the type of hydrodynamic expansion, we have made a confusion matrix analysis whose results are shown in figure 5. The rows of the matrix correspond to the outcome of the full computation, whereas the columns give the prediction of the analytic formula. The last row corresponds to points for which a steady-state solution was not found. The numerical values of each cell are normalized to the total number of points in the scan.

In the language of the confusion matrix for multi-class classification, the diagonal elements represent the fraction of times the analytic prediction classified the solution correctly, and the off-diagonal matrix elements the fraction of times it misclassified them. We can see that the formula classified incorrectly about 15% of the points as detonations when in fact they were hybrids, see the 23 matrix element. We made use of the `scikit-learn` python package [127] for the evaluation of the confusion matrix elements and obtained a total weighted F-score of $F_1 = 0.8$, which is obtained from the harmonic mean of the precision. We recall that the best possible F-value is 1 and poorest F-value is 0.

6 Gravitational waves

The computation of the gravitational wave spectrum relies on estimates for the thermodynamic parameters of the FOPT. One of these key parameters, the percolation temperature, was already discussed in the previous section, and we introduce the three remaining parameters in this section.

JHEP01(2023)093

The strength of the phase transition is proportional to the trace anomaly, i.e.,

$$\alpha \equiv \frac{1}{4\rho_r}\Delta \mathrm{Tr}T^{\mu}_{\nu} = \frac{1}{\rho_r}\left(\Delta V_{\mathrm{eff}}(\phi,T) - \frac{T}{4}\Delta\frac{\partial V_{\mathrm{eff}}(\phi,T)}{\partial T}\right), \tag{6.1}$$

where Δ denotes the differences between quantities in the false and true minima. Another relevant parameter, denoted by β, defined by

$$\frac{\beta}{H} \equiv T_*\frac{d}{dT}\left(\frac{S_3}{T}\right)\Big|_{T=T_*}, \tag{6.2}$$

specifies the inverse time duration of the phase transition. We evaluate the GW spectrum at the temperature reached after the transition when the vacuum energy is converted into radiation:

$$T_* = T_p(1+\alpha(T_p))^{1/4}. \tag{6.3}$$

The final relevant parameter is the wall velocity v_w, which we discussed in detail in section 5. Here we will use the results of our detailed numerical analysis although, as we have shown, the analytic estimate from eq. (5.1) would yield very similar results.

Since the potential is polynomial, we do not expect significant supercooling [103], which implies that the bubbles will not become very energetic [128–132]. Hence we can focus exclusively on GWs sourced by plasma motion [6, 7]. Despite significant progress in the modelling of turbulence [133–136], the calculation of GWs from its emergence after a phase transition remains uncertain, and we will omit this source. This leaves us with sound waves as the main source, for which we use the results of lattice simulations to compute the GW signal [137–140]:

$$\Omega_{\mathrm{sw}}(f)h^2 = 4.13\times10^{-7}\,(R_*H_*)\left(1-\frac{1}{\sqrt{1+2\tau_{\mathrm{sw}}H_*}}\right)\left(\frac{\kappa_{\mathrm{sw}}\,\alpha}{1+\alpha}\right)^2\left(\frac{100}{g_*}\right)^{\frac{1}{3}}S_{\mathrm{sw}}(f), \tag{6.4}$$

where

$$S_{\mathrm{sw}}(f) = \left(\frac{f}{f_{\mathrm{sw}}}\right)^3\left[\frac{4}{7}+\frac{3}{7}\left(\frac{f}{f_{\mathrm{sw}}}\right)^2\right]^{-\frac{7}{2}}, \tag{6.5}$$

the frequency of the peak is given by

$$f_{\mathrm{sw}} = 2.6\times10^{-5}\mathrm{Hz}\,(R_*H_*)^{-1}\left(\frac{T_*}{100\mathrm{GeV}}\right)\left(\frac{g_*}{100}\right)^{\frac{1}{6}}, \tag{6.6}$$

and g_* is the number of degrees of freedom at T_*, which we compute using the results of [102]. In order to approximate the duration of the sound wave period normalised to the Hubble rate we use [103, 128, 139, 141, 142]

$$\tau_{\mathrm{sw}}H_* = \frac{H_*R_*}{U_f}, \quad U_f \approx \sqrt{\frac{3}{4}\frac{\alpha}{1+\alpha}\kappa_{\mathrm{sw}}}, \tag{6.7}$$

and to approximate the average bubble radius, again normalised to the Hubble rate, we use

$$H_*R_* \approx (8\pi)^{\frac{1}{3}}\,\mathrm{Max}(v_w,c_s)\left(\frac{\beta}{H}\right)^{-1}, \tag{6.8}$$

JHEP01(2023)093

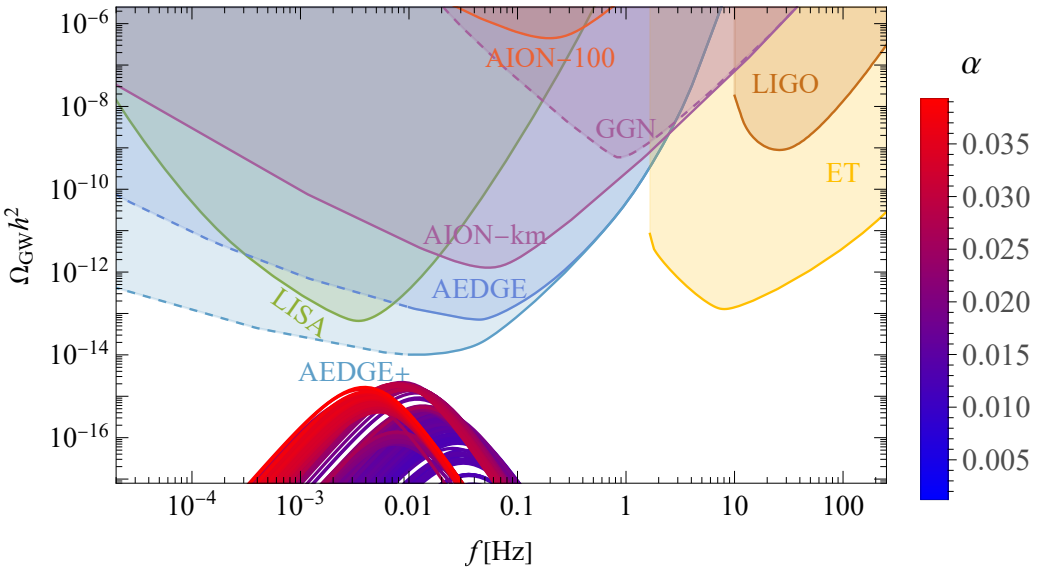

Figure 6. Gravitational wave spectra from points with bubble walls that are not very relativistic, for which we find hydrodynamical solutions.

where we use the duration of the transition given in eq. (6.2). Finally, we use the fluid velocity and temperature profiles discussed in section 3 of ref. [94] to calculate the sound wave efficiency factor as the energy converted into bulk fluid motion, which is given by [126]

$$\kappa_{sw} = \frac{3}{\alpha\,\rho_{\rm R}\,v_w^3}\int w\,\xi^2\frac{v^2}{1-v^2}d\xi = \frac{4}{\alpha\,v_w^3}\int\left(\frac{T(\xi)}{T_p}\right)^4\xi^2\frac{v^2}{1-v^2}d\xi\,. \tag{6.9}$$

The signal-to-noise ration observed by a given experiment is given by

$$\text{SNR} \equiv \sqrt{T}\left[\int_{f_{\rm min}}^{f_{\rm max}}\left(\frac{\Omega_{\rm sw}(f)}{\Omega_{\rm noise}(f)}\right)^2 df\right]^{1/2}\,, \tag{6.10}$$

which we calculate assuming the duration of each mission to be $T = 4$ years. We visualise the sensitivities of experiments using the standard power-law integrated sensitivities [143].

We show the spectra from our scans in figures 6 and 7, with the first one showing only points for which we were able to compute the wall profile and velocity, while in the second one the friction was not enough for the walls to reach a steady state and we assumed $v_w \approx 1$ instead. Both figures also show the design sensitivity of the currently running LIGO [143–146] and future interferometers LISA [147, 148] and ET [149, 150] as well as proposed devices based on atom interferometry [9], AION-1km [151] and AEDGE [8]. We do not include the impact of the GW foreground produced by the population of BH currently probed by LIGO and Virgo [152]. This effect would likely further limit our detection prospects, however, it would not change our conclusions. We see only points where the wall velocity is close to unity and do not find hydrodynamical solutions that produce signals strong enough to be observed in upcoming experiments. This trend follows similar observations made in the SMEFT and the $\mathbb{Z}_2$-symmetric versions of the model [93, 94].

JHEP01(2023)093

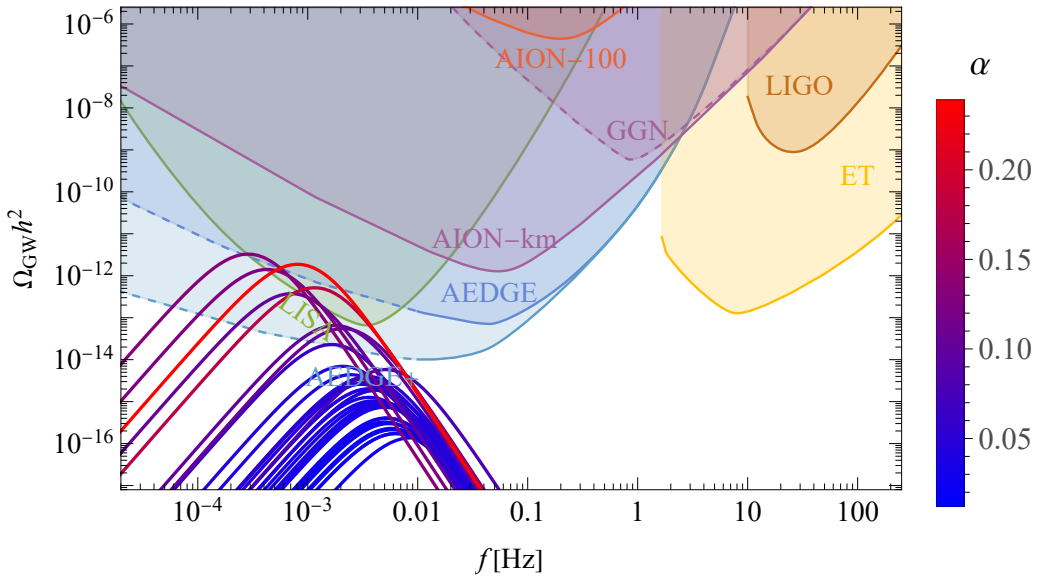

Figure 7. Gravitational wave spectra from points in the parameter space for which the transitions are too strong and we do not find hydrodynamical solutions. Here we simply assume $v_w \approx 1$. We note that these points are not suitable for baryogenesis.

Significant progress has been made recently on hybrid calculations of GW generation by sound waves, which shows non-trivial dependence of the shape of the spectrum on the wall velocity [153–156]. However, these modifications do not have a large impact on the peak GW density. They would only modify the spectra in figure 6 when the velocities are non-relativistic. As the spectra in such cases are too weak to be observed in future experiments, the overall impact of these updates on upcoming searches are not expected to be very significant in the model studied here.

7 Baryogenesis

We discuss in this section the use of the CP-violating dimension-5 operator

$$\mathcal{L} \supseteq y_t \bar{Q}\tilde{\Phi}t_R\left(i\frac{s}{\Lambda_{\rm CP}}\right) + \text{h.c.} \tag{7.1}$$

to achieve baryogenesis in the general singlet extension of the SM discussed in section 2.[5] The baryon asymmetry that can be generated by this operator has been investigated previously, mostly in the singlet extension with a $\mathbb{Z}_2$-symmetric potential and vanishing vev [93, 94]. Here we first review the phenomenological constraints on this model before exploring the possible magnitude of the baryon asymmetry that it can generate in the presence of a zero-temperature vev u, under various conditions.

[5] A related dimension-6 six operator, i.e., with $s/\Lambda_{\rm CP} \to s^2/\Lambda^2_{\rm CP}$, was considered in [17, 78] as a possible term in a $\mathbb{Z}_2$-symmetric theory.

JHEP01(2023)093

7.1 Higgs signal strengths and CP properties

In the presence of the operator (7.1), the top quark mass deviates from the SM expression $m_t = y_t^{\rm SM} v/\sqrt{2}$ when the singlet develops a zero-temperature vev u. Hence the top-quark Yukawa coupling y_t must be rescaled accordingly:

$$y_t = \frac{y_t^{\rm SM}}{\sqrt{1+\frac{u^2}{\Lambda_{\rm CP}^2}}} = \frac{m_t\sqrt{2}}{v\sqrt{1+\frac{u^2}{\Lambda_{\rm CP}^2}}} \tag{7.2}$$

in order to reproduce correctly the top-quark mass value obtained from Tevatron and LHC measurements (see, e.g., [157]), for which we use the Particle Data Group value $m_t = 172.9\,\text{GeV}$ [158].

In parallel, singlet-doublet mixing through the angle θ,[6] reduces universally the couplings of the Higgs boson to SM particles by a factor $\cos\theta \equiv c_\theta$. In the specific case of the top quark, this reduction combines with the modification of the Higgs-top coupling induced by the effective operator (7.1) to yield a Higgs-top interaction $(m_t/v)\, h\, \bar{t}\,(\kappa_t + i\,\tilde{\kappa}_t\,\gamma_5)\, t$, where

$$\kappa_t = \frac{c_\theta}{\sqrt{1+\frac{u^2}{\Lambda_{\rm CP}^2}}}\,, \quad \tilde{\kappa}_t = \frac{c_\theta\frac{u}{\Lambda_{\rm CP}} - s_\theta\frac{v}{\Lambda_{\rm CP}}}{\sqrt{1+\frac{u^2}{\Lambda_{\rm CP}^2}}}\,. \tag{7.3}$$

The corresponding coupling modifier w.r.t. the SM value is $|g_{htt}| = \sqrt{\kappa_t^2+\tilde{\kappa}_t^2}$. These effects impact the predictions for Higgs signal strength measurements at the LHC and their interpretation.[7] We have performed a χ^2 fit to the latest Higgs signal strength measurements published by ATLAS in its $10^{\rm th}$-year Higgs Legacy analysis [159],[8] in terms of the parameters s_θ and $u/\Lambda_{\rm CP}$. The $2\,\sigma$ ($\Delta\chi^2 = 6.18$) allowed regions for different values of the singlet vev u are enclosed by the solid lines in the left panel of figure 8, distinguishing the cases of positive and negative u. In addition, a recent CMS analysis has constrained the CP structure of the Higgs-top interaction [161], yielding the $2\,\sigma$ bound $\tilde{\kappa}_t^2/(\kappa_t^2+\tilde{\kappa}_t^2) < 0.669$, and the corresponding allowed region of the $(s_\theta,\, u/\Lambda_{\rm CP})$ plane lies within the dashed contours in figure 8 (left). However, we find that this bound on the Higgs CP properties is weaker that from Higgs signal strength measurements throughout the entire parameter space of the model. The coloured points in figure 8 (left) are those selected for our baryogenesis analysis in section 7.5, and we see that they are all comfortably consistent with the constraints from LHC Higgs Signal Strengths.

7.2 Electroweak precision observables

In general, the extra scalar in our model makes corrections to the gauge boson self-energy diagrams. The leading effects on the electroweak precision observables (EWPOs) are

[6] Hereafter we use the notations h and s for the mass eigenstates that are predominantly Higgs and singlet, respectively.

[7] We do not discuss here constraints from Higgs self-coupling measurements, which are currently relatively weak.

[8] The corresponding Higgs signal strength analysis by CMS [160] cannot be reinterpreted in our framework, so we do not include it in our χ^2 fit.

JHEP01(2023)093

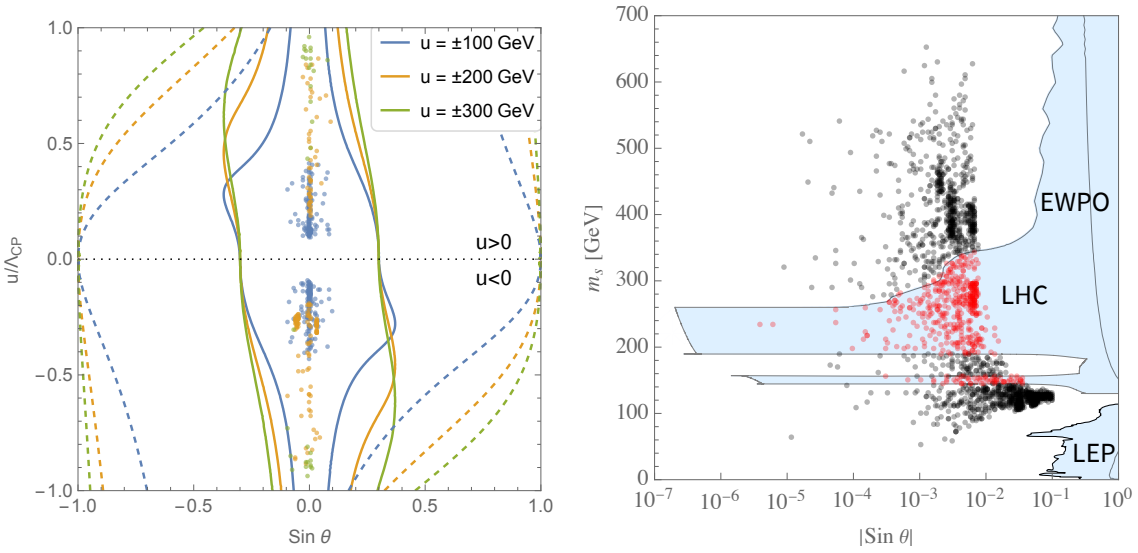

Figure 8. Left: 2-σ allowed regions in the $(\sin\theta, u/\Lambda_{\rm CP})$ plane for different values of the singlet vev u, from a χ^2 fit to the Higgs signal strength measurements from ATLAS in its $10^{\rm th}$-year Higgs Legacy paper [159] (solid lines), and from a measurement of the CP structure of the $h\bar{t}t$ coupling by CMS [161] (dashed lines). Right: the $(\sin\theta, m_s)$ plane showing regions excluded at the 2-σ level by LEP searches for light singlet-like scalars, LHC searches, and measurements of EW precision observables. The points selected for our baryogenesis analysis in section 7.5 are shown in black on the right panel (the red points are excluded by LHC searches), and in colours corresponding to the indicated values of $u \pm 5\%$ in the left panel.

described by the oblique parameters S, T and U. Since the new scalar is electrically neutral, only the W and Z boson self-energies receive corrections at the leading order. Complete expressions for the shifts in the oblique parameters from their SM values, $\Delta S, \Delta T$ and ΔU, are given at 1-loop order ref. in [33]. The respective numerical values of $\Delta S, \Delta T$ and ΔU obtained from a global fit to EWPO measurements [162] are

$$\Delta S = 0.04 \pm 0.11,\ \Delta T = 0.09 \pm 0.14,\ \Delta U = -0.02 \pm 0.11\,, \tag{7.4}$$

together with the correlation coefficients $+0.92$ between ΔS and ΔT, -0.68 between ΔS and ΔU and -0.87 between ΔT and ΔU. We then build the correlation matrix and use the χ^2 implementation procedure described in [33]. The region of the $(\sin\theta, m_s)$ plane excluded at the 2 σ level is shaded blue in the right panel of figure 8.[9]

7.3 LEP and LHC searches for BSM scalars

The Higgs searches at LEP yield constraints on the singlet-doublet mixing angle θ for light singlet masses, $m_s \lesssim 100\,\text{GeV}$ (see e.g. [164]), depicted in the right panel of figure 8 in the $(\sin\theta,\ m_s)$ plane. Figure 8 highlights that the LEP Higgs bounds do not yield relevant constraints on the parameter points of our scan, which are shown in black in the right panel of figure 8.

[9] Our analysis does not include recent experimental measurements of M_W, which are discussed in [163].

JHEP01(2023)093

In addition, BSM scalar searches at the LHC in WW, ZZ and hh decay channels constrain the properties of the singlet-like scalar state s for $m_s > m_h$. For $m_s > 200\,\text{GeV}$, the strongest such limits have been obtained by ATLAS in the $ZZ \to 4\ell$ and $ZZ \to 2\ell\,2\nu$ final states [165] with $\sqrt{s} = 13\,\text{TeV}$ LHC data and $139\,\text{fb}^{-1}$ of integrated luminosity. In order to interpret these bounds in our setup, we note that the effective operator (7.1) impacts both gluon-gluon fusion production, $gg \to s$, and the partial decay width of the singlet-like scalar into top quarks $s \to t\bar{t}$, when phase space is available. The strength of the interaction between the scalar s and the top quark relative to that of the Higgs-top coupling in the SM is given by

$$|g_{stt}| = \frac{1}{\sqrt{1+\frac{u^2}{\Lambda_{\text{CP}}^2}}}\sqrt{s_\theta^2 + \left(\frac{u\,s_\theta}{\Lambda_{\text{CP}}} + \frac{v\,c_\theta}{\Lambda_{\text{CP}}}\right)^2}\,, \tag{7.5}$$

where $s_\theta \equiv \sin\theta$ and $c_\theta \equiv \cos\theta$. We note that $|g_{stt}| \to (v/\Lambda_{\text{CP}}) \times 1/\sqrt{1+(u/\Lambda_{\text{CP}})^2}$ in the limit $\sin\theta \to 0$, so the singlet production cross section does not vanish in this limit, because of the operator (7.1) that is postulated for baryogenesis. Therefore LHC searches may be sensitive to very small singlet-doublet mixing, if the value of Λ_{CP} is close to the TeV scale. At the same time, we stress that if the $s \to t\bar{t}$ decay is kinematically accessible[10] it becomes the dominant scalar branching fraction in the $\sin\theta \ll 1$ limit, suppressing the signal in $s \to ZZ$ searches. In such a case, the bounds from $pp \to s \to ZZ$ searches at the LHC become independent of the values of u and Λ_{CP}, since the dependence on $|g_{stt}|$ approximately cancels in the limit of $\sin\theta \ll 1$ between $\sigma_{pp\to s} \propto |g_{stt}|^2$ and $\text{BR}_{s\to ZZ} \propto |g_{stt}|^{-2}$. For scalar masses $m_s < 200\,\text{GeV}$, LHC search results for $s \to WW, ZZ$ with $\sqrt{s} = 13\,\text{TeV}$ data are available from CMS [166], with a smaller ($35.9\,\text{fb}^{-1}$) integrated luminosity.[11] However, these still provide strong constraints in the mass region $130\,\text{GeV} < m_s < 200\,\text{GeV}$, where the ATLAS search [165] mentioned above does not apply.

The 2-σ limits from BSM scalar searches at the LHC in WW and ZZ decay channels in the ($\sin\theta$, m_s) plane are shown in the right panel of figure 8, with the points in our scan that are excluded by these LHC searches coloured red. We note that s may become long-lived in the limit of very small singlet-doublet mixing when the s decay into top quarks (including the three-body decay $s \to t\,W\,b$) is kinematically forbidden, corresponding to $m_s \lesssim 260\,\text{GeV}$, in which case the above $s \to ZZ$ limits from prompt LHC searches are evaded. Considering that the singlet scalar is typically produced with 3-momentum $|\vec{p}_s| \lesssim m_s$ (in the ATLAS/CMS detector frame) and the decay of s ceases to be prompt for a decay-length $c\tau_s \gtrsim \mathcal{O}(\text{mm})$, the ATLAS bounds from [165] and CMS bounds from [166] are evaded for $\sin\theta \lesssim 10^{-6} - 10^{-7}$ (with the specific value decreasing as m_s increases), as we depict in the right panel of figure 8.

Finally, regarding future LHC searches, we stress that an increase in the sensitivity of searches for new scalars with $m_s < 200\,\text{GeV}$ in di-boson final states (at present only the

[10] We note that for very small mixing angles $\sin\theta < 0.01 - 0.001$ the three-body decay of s via an off-shell (anti)top (open for $m_s \gtrsim m_t + m_W + m_b$) can still dominate over the WW and ZZ decays, whose partial widths are suppressed by $\sin^2\theta$ w.r.t. their SM-like values.

[11] LHC $s \to WW, ZZ$ searches with $\sqrt{s} = 7$ and $8\,\text{TeV}$ data [167, 168] yield much weaker constraints and do not affect the parameter points from our baryogenesis scan.

JHEP01(2023)093

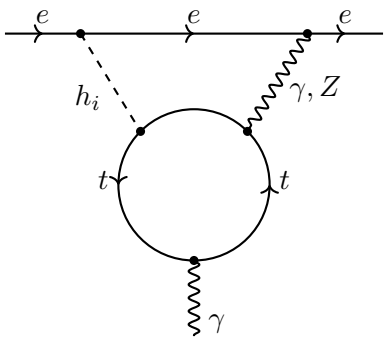

Figure 9. The 2-loop Bar-Zee diagram that contributes to the electron electric dipole moment [169]. Here h_i denotes the mass eigenstates h and s.

aforementioned CMS search [166] with $\sqrt{s} = 13\,\text{TeV}$ LHC data exists) could have the capability to explore fully the viable baryogenesis parameter space that remains unconstrained in the model. In particular, an estimate of the HL-LHC sensitivity in this mass region via a naive rescaling of the current CMS limits from [166] by the square-root of the ratio of integrated luminosities indicates that mixing angles down to the long-lived singlet scalar case $\sin\theta \sim 10^{-6}$ could be probed in this mass range.

7.4 The electron electric dipole moment

The effect of the dim-5 operator on the electron electric dipole moment (eEDM) is given by the 2-loop Bar-Zee diagram [169] with a top quark loop, see figure 9, whose contribution is given by the following formula [170]:

$$d_e^{2-\text{loop}} = \frac{e}{3\pi^2}\frac{\alpha G_F v}{\sqrt{2}\pi m_t} m_e \left(\frac{v}{\sqrt{2}\Lambda_{\text{CP}}}\right) \sin\theta\cos\theta \left[-g\left(\frac{m_t^2}{m_h^2}\right) + g\left(\frac{m_t^2}{m_s^2}\right)\right], \tag{7.6}$$

with the 1-loop integral

$$g(z) = \frac{z}{2}\int_0^1 dx \frac{1}{x(1-x)-z}\log\left[\frac{x(1-x)}{z}\right]. \tag{7.7}$$

We see in the above expression that the prediction for the eEDM depends only on θ, m_s and the cutoff scale Λ_{CP}, and in particular it vanishes in the limit of vanishing mixing angle $\theta \to 0$ or scalar mass degeneracy $m_s \to m_h$.

We use the following numerical values for the physical constants [158] in the formula for the eEDM:

$$\begin{aligned} e \equiv g' &= 0.34\,, \\ \alpha &= 1/137\,, \\ G_F \equiv \frac{1}{\sqrt{2}v^2} &= 1.166 \times 10^{-5}(\text{GeV})^{-2}\,, \\ m_e &= 0.5\,\text{MeV}\,, \\ m_t &= 172.9\,\text{GeV}\,. \end{aligned} \tag{7.8}$$

JHEP01(2023)093

The best current experimental upper bound on the eEDM, obtained by the ACME collaboration [171], is

$$|d_e| < 1.1 \times 10^{-29} e\,\mathrm{cm} = 1.89 \times 10^{-16}\,\mathrm{GeV}^{-1}\,. \tag{7.9}$$

7.5 The baryon asymmetry

Although the above formula for the field-dependent top quark mass might seem like a minor modification of the scalar potential, it can nevertheless have a significant numerical impact on the thermodynamic parameters of the transition, and must be taken into account. These effects have not been considered in previous studies. Instead, it has been customary to neglect altogether the impact that the mixing with the scalar in eq. (7.1) has on the phase transition and to solve for the value of $\Lambda_{\rm CP}$ that yields the required BAU. We note in addition that the dependence of the top quark mass on the singlet profile induces a friction term, $F_{\rm friction} \propto dm_t/ds$, in the singlet equation of motion. However, we have verified that the numerical impact of this term is irrelevant.

Since the above modifications lead to a different scalar potential from that studied in the preceding sections, we have performed an independent scan of the parameter space with the above modified effective potential, treating $\Lambda_{\rm CP}$ as one of its parameters, using the eEDM constraint as a filter and incorporating all the phenomenological constraints. We find that the new effective potential always develops a global minimum with $(h, s) = (v, u)$ that is distinct from that at the electroweak scale, but that its location in field space is several orders of magnitude beyond the Planck scale. Hence we do not consider this prospective destabilization to be a serious concern.

To compute the baryon asymmetry of the Universe (BAU) we use the improved fluid equations of ref. [91], which are well behaved for any value of the wall velocity. We have scanned over parameter values uniformly distributed in the following ranges:

$$\begin{aligned} m_s &\in [1, 1000]\,\mathrm{GeV}\,, \\ \theta &\in [-0.1, 0.1]\,, \\ \Lambda_{\rm CP} &\in [v, 1000]\,\mathrm{GeV}\,, \\ u &\in [-1000, 1000]\,\mathrm{GeV}\,, \\ \mu_3 &\in [-1000, 1000]\,\mathrm{GeV}\,, \\ \mu_{hs} &\in [-1000, 1000]\,\mathrm{GeV}\,. \end{aligned} \tag{7.10}$$

As discussed above, we have checked that all the points are consistent with the phenomenological constraints, and that $\Lambda_{\rm CP}$ is the highest mass scale, so that the effective field theory is always consistent. The results for the full computation are presented in figure 10 as functions of the wall velocity v_w and the strength parameter α_0 (coloured in the left panel according to the value of h_0), which are the parameters with the most significant impact. As indicated, the BAU η is positively correlated with the wall velocity and with the Higgs bubble profile amplitude, in agreement with the findings in [94]. We see that η can attain its observed value today most easily when the wall expansion is hybrid.

The positive correlation exhibited in figure 10 above might look at odds with the results of ref. [91] which displayed instead a negative correlation between the BAU and the wall

JHEP01(2023)093

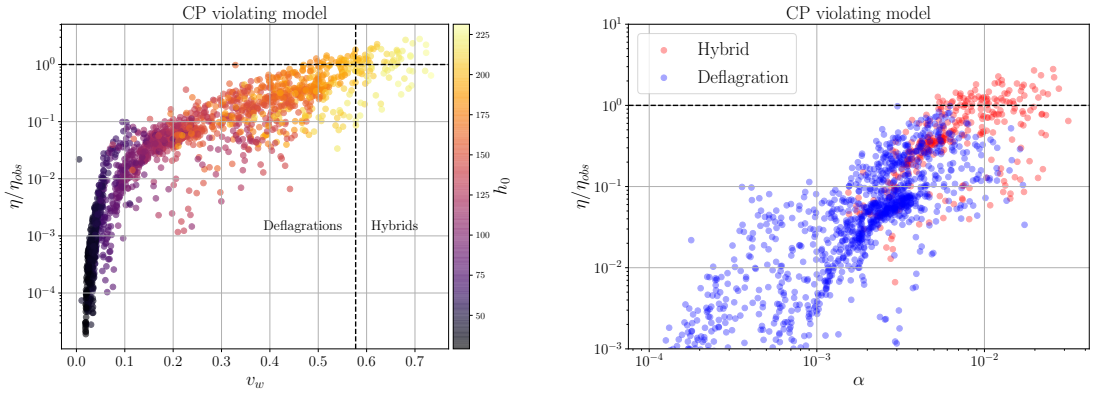

Figure 10. Results for the baryon asymmetry of the Universe (BAU) normalized to its observed value as a function of the wall velocity (left panel) and the strength α_0 of the phase transition (right panel). The coloured side-bar alongside the left panel indicates the value of the Higgs bubble profile amplitude h_0.

velocity, see figure 3 in that reference.[12] The reason for this apparent contradiction is that figure 3 in [91] was produced by fixing all parameters of the transition except the wall velocity. Computing solutions from first principles we find all the other parameters must also be different to obtain solutions with a different wall velocity. The premise of [91] is the separation of the fluid equations into CP-conserving and CP-violating components with the latter being used to compute the baryon yield and with the former for the properties of the wall. As we have demonstrated in the preceding sections, the properties of the wall are intimately connected with one another when computed from first principles in a specific model. Furthermore, it was shown in [94] that solving the CP-violating equations using the thermodynamic variables in front of the wall, i.e., v_+, T_+, induces an extra enhancement of the baryon asymmetry as a function of velocity, though no physical intuition for this effect was provided in that reference.

We now aim to clarify this situation by comparing a simplified fiducial model with a more realistic example capturing the dependence on the wall velocity and mimicking the hydrodynamic effects of the plasma. For the fiducial model we take

$$h_0 = \frac{s_h}{2} = T_n = 100\,\text{GeV}, \qquad \Lambda_{\text{CP}} = 1\,\text{TeV},$$
$$L_h = L_s = \frac{5}{T_n}, \qquad s_l = \delta_s = 0, \tag{7.11}$$

which is similar to the benchmark model used in [91]. To incorporate the wall velocity-dependence of the width we make use of the results of section 5. From the parameter scan we found that to a good approximation

$$T_+ L_h \approx T_+ L_s \approx \frac{5}{v_w}, \tag{7.12}$$

[12] See in addition figures 1, 2 of ref. [172], which used a different set of fluid equations with higher-order moments.

JHEP01(2023)093

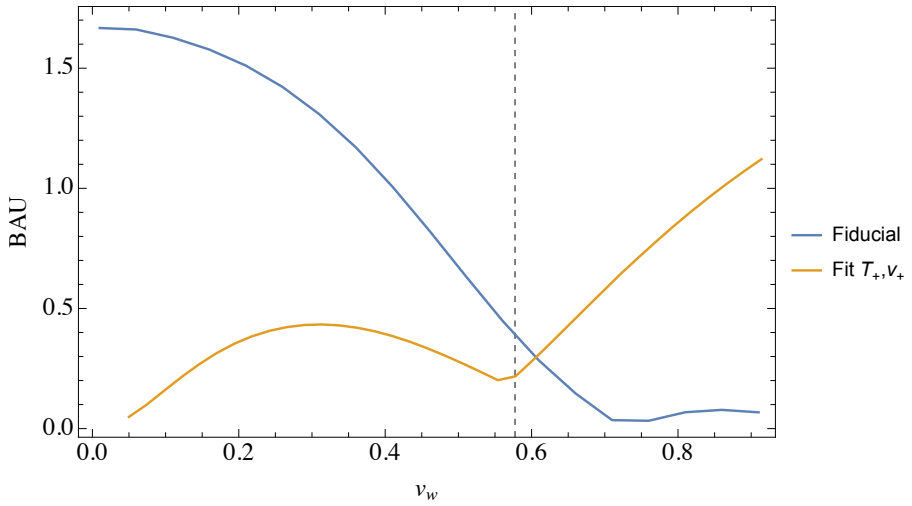

Figure 11. Baryon yield as a function of velocity for the fiducial point (7.11) and using the fits of eqs. (7.12) and (7.13).

where $T_+ \approx T_n$ is the temperature just in front of the wall and the heating is not a strong effect since the strength parameter α is very small. Similarly, the fluid velocity in front of the wall can be fitted as

$$v_+ \approx \begin{cases} v_w, & v_w \leq c_s, \\ \frac{0.32}{v_w}, & v_w > c_s \end{cases} \tag{7.13}$$

where, again, one normally expects $v_+ < v_w$ for deflagrations and hybrids but the effect is not strong enough since the transitions are very weak. Only for hybrids do we start seeing a noticeable deviation. We compare in figure 11 the output of these two implementations, noticing that the fiducial curve closely matches figure 3 of [91]. On the other hand, the curve obtained from the fit clearly shows a sustained growth for low and high ($v_w > c_s$) velocities. The drop in the middle region can be attributed to the velocity dependences of other properties of the wall, e.g., the profile amplitudes which we do not consider. In summary, the baryon asymmetry is enhanced for faster walls (within deflagrations and hybrids) because 1) faster walls are thinner and 2) the fluid velocity in front of the wall decreases [173] and one has $\eta \propto 1/v_+$ [91].

In analogy with our results for the bubble wall properties shown in the previous section, we show in figure 12 the results for the CP-violating model. We see that the range of the strength parameter α is significantly smaller than in the generic model without CP violation. As a consequence, the analytic formula yields underestimates for all the points and, as we saw in figure 4, the relative error is significant. Because of the low values of α, the GW signal is too small to be measured in planned experiments. In summary: when the properties of the wall are calculable the GW signals are not strong enough to be measurable in forthcoming experiments, and the GW spectra in the models with and without CP violation look very similar.

JHEP01(2023)093

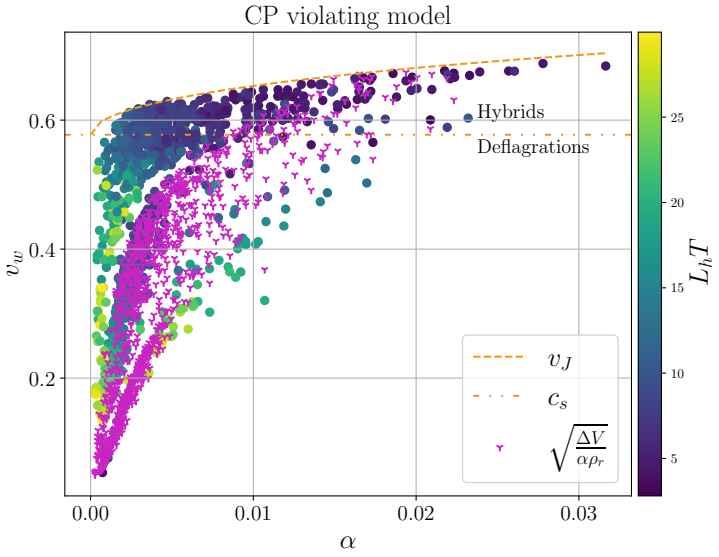

Figure 12. The wall velocity as a function of the strength parameter α for the CP-violating model. The lines and the colour coding of the points are the same as in figure 3.

It is well known that in the SM the perturbative effective potential develops an instability at a scale $\sim 10^{12}$ GeV induced by the negative renormalization of the Higgs quartic coupling that is induced by the top quark Yukawa coupling. Therefore the rescaling of the top Yukawa rescaling raises a natural question: what is the impact of this rescaling on the stability and perturbativity of the potential at higher energy scales? A dedicated answer lies beyond the scope of the present paper, but we have investigated this question using the 1-loop renormalization group equations, as described in an appendix. As seen in figure 13, we have found that only a modest number of points (coloured red) are ruled out because instability sets in below $\Lambda_{\rm CP}$, that there are many points which are no more unstable than the SM, and that there are a sizeable fraction of points that are stable and theoretically consistent up to the Planck scale.

Finally, we display in the left panel of figure 14 the parameter space in the plane of singlet mass m_s and Higgs portal coupling λ_{hs} that is consistent with all experimental data and with a non-zero $\eta \neq 0$, and in the right panel we show the allowed parameter space in the $(\sin\theta, m_s)$ plane. The sparseness of the sample for $190\,\text{GeV} \lesssim m_s \lesssim 300\,\text{GeV}$ and in the small region around $m_s \sim 150\,\text{GeV}$ is due to the impact of the LHC constraints. The orange points give η within 10% of the observed value today and thus constitute the most successful predictions found in the present study. The relatively small mass of the s boson for such scenarios, $m_s \lesssim 150\,\text{GeV}$, is within the kinematic reach of the LHC for singlet-like scalar production in association with a $\bar{t}t$ pair, and will be also probed by future LHC searches in di-boson final states. We also note that increasing the precision of the eEDM experiment by an order of magnitude (as expected by the ACME Collaboration in the future [171, 174]) would be sensitive to around 75% of our sample of points that yield the right baryon abundance. In contrast, as already mentioned, the GW signal is too small to be observable.

JHEP01(2023)093

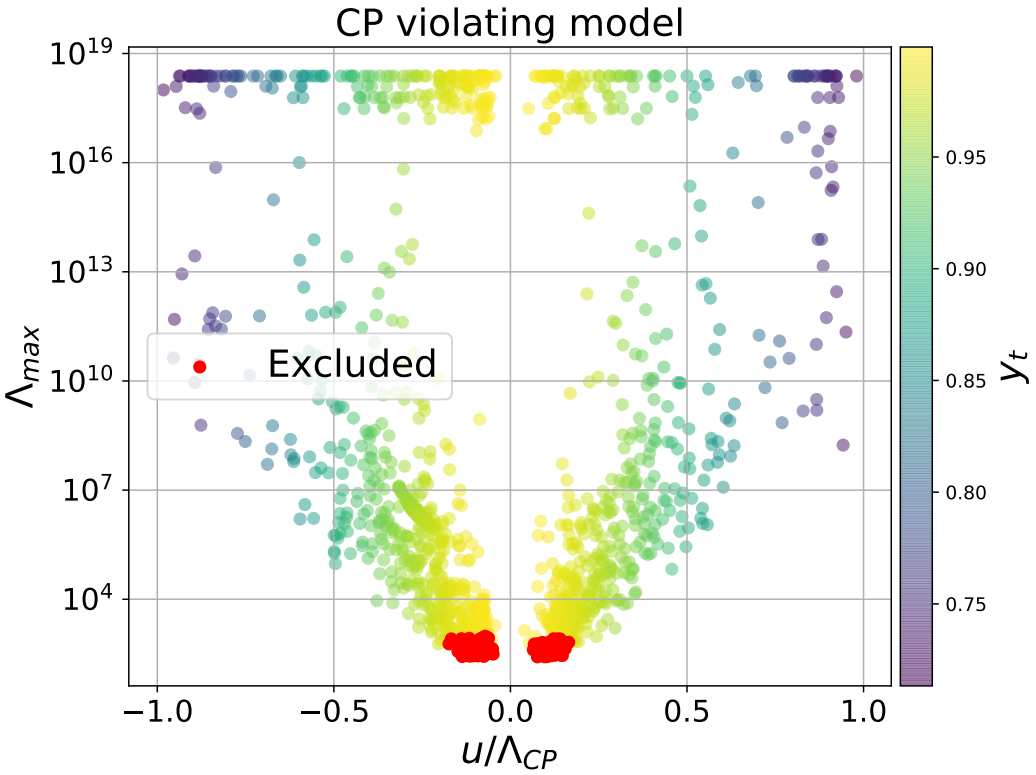

Figure 13. Maximum renormalization scale where positivity and perturbativity are satified as a function of $u/\Lambda_{\rm CP}$. The coloured side-bar shows the value of the top Yukawa coupling.

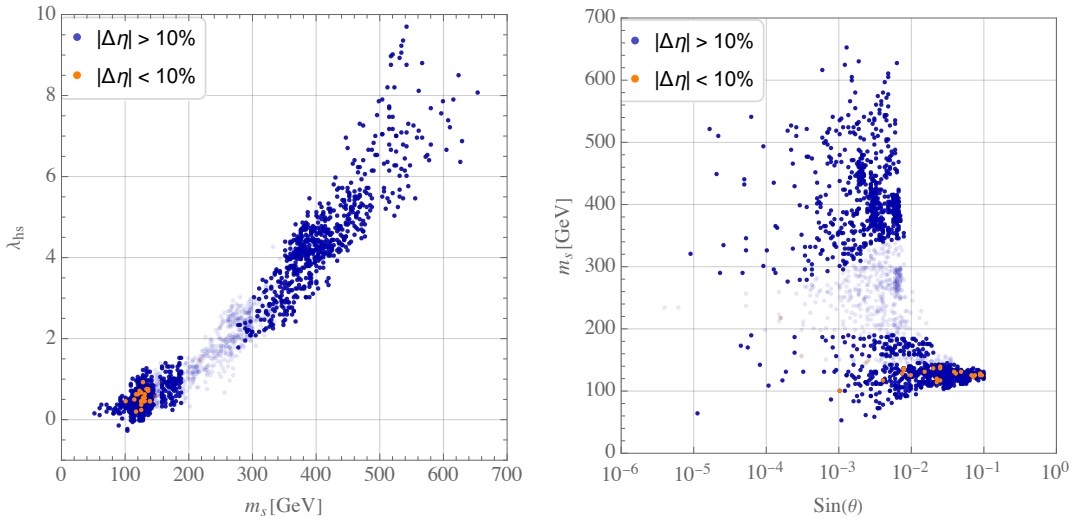

Figure 14. Allowed parameter space of the CP-violating singlet model in the (m_s, λ_{hs}) plane (left panel) and the $(\sin\theta, m_s)$ plane (right panel). The orange points predict a baryon asymmetry that lies within 10% deviation of the cosmological value, and hence delimit the preferred region.

JHEP01(2023)093

8 Conclusions

We have revisited in this paper the extension of the SM with one additional gauge singlet scalar field, allowing the $\mathbb{Z}_2$ symmetry of the potential to be broken. We have considered both the case where the symmetry is broken spontaneously and the more general case in which the potential is extended with extra terms and the symmetry breaking is explicit. We have investigated details of the electroweak phase transition in the different cases, with the aim of estimating the possible magnitude of the gravitational wave signal, assessing the possibility of realising electroweak baryogenesis, and investigating whether they can coexist.

In the case with spontaneous breaking we find that after inclusion of the full one-loop potential the transitions are always weak, i.e., $v/T \lesssim 1$, which gives little hope for electroweak baryogenesis. The case with explicit symmetry breaking is more promising, and may give rise to a transition strong enough for baryon production. We investigate the bubble wall properties, using the semiclassical fluid equations to calculate the final velocity and shape of the wall. This allows us to compute accurately the baryon yield, for which we use a dimension-five operator that couples the singlet scalar to the SM top quarks, yielding a new source of CP violation. Despite stringent constraints from the experimental limits on the electron dipole moment and from direct searches for singlet-like scalars at the LHC, we find that a significant part of the allowed parameter space produces a baryon yield close to the observed value. Such regions of parameter space are within reach of upcoming LHC searches, and could also be probed in the future by an $\mathcal{O}(10)$ increase in the sensitivity of electron electric dipole moment experiments.

However, just as in other simple SM extensions [93, 94], we find that all the transitions capable of producing an appreciable baryon yield result in GW signals that are too weak to be observed in upcoming experiments. The reason is that, already for weak transitions with $\alpha \approx 0.05$, the vacuum pressure becomes sufficiently large that the wall is not stopped in our semiclassical fluid picture. To be more precise, there is a distinction between weak transitions for which the hydrodynamical solution is such that the plasma is heated in front of the wall and stronger transitions that predict a so-called detonation solution in which the plasma outside the wall has the same temperature as before the transition. If the transition is strong enough that the heated plasma shell outside the wall disappears the friction drops substantially and there is no solution up to very large wall velocities where the semi-classical fluid approximation breaks down. This means that for such strong transitions the wall will reach a velocity close to the speed of light and the hope of realising electroweak baryogenesis fades. Because the division between the two cases is at such small transition strength, we find that only transitions with relativistic walls predict observable gravitational wave signals.

As a by-product we provide an analytical approximation for the wall velocity which does not require any additional computation beyond those of the standard thermodynamics parameters used when approximating the GW signal. We have compared this approximation with our detailed numerical results, and find that it gives results that are typically accurate with within a few percent. We also find it to be accurate for separating the solutions between those with slow walls that are appropriate for baryogenesis and those with relativistic walls that give strong GW signals.

JHEP01(2023)093

Acknowledgments

We would like to thank Bogumiła Świeżewska for comments on the manuscript. The work of JE was supported in part by United Kingdom STFC Grants ST/P000258/1 and ST/T000759/1, and in part by the Estonian Research Council via a Mobilitas Pluss grant. The project is co-financed by the Polish National Agency for Academic Exchange within Polish Returns Programme under agreement PPN/PPO/2020/1/00013/U/00001 and the Polish National Science Center grant 2018/31/D/ST2/02048. The work of J.M.N. is supported by the Ramón y Cajal Fellowship contract RYC-2017-22986, and by grant PGC2018-096646-A-I00 from the Spanish Proyectos de I+D de Generación de Conocimiento. J.M.N. also acknowledges support from the European Union's Horizon 2020 research and innovation programme under the Marie Sklodowska-Curie grant agreement 860881 (ITN HIDDeN), as well as from the grant IFT Centro de Excelencia Severo Ochoa CEX2020-001007-S funded by MCIN/AEI/10.13039/501100011033.

A One-loop analysis of positivity and perturbativity

The beta functions in the most generic scalar singlet extension without $\mathbb{Z}_2$ symmetry have been studied in ref. [175] in the context of vacuum stability and positivity. In this paper we are only concerned about positivity and perturbativity of the quartic couplings, thus the relevant RGE system at 1-loop is given by

$$16\pi^2\beta_{g_1} = \frac{41}{6}g_1^3, \tag{A.1}$$

$$16\pi^2\beta_{g_2} = -\frac{19}{6}g_2^3, \tag{A.2}$$

$$16\pi^2\beta_{g_3} = -7g_3^3, \tag{A.3}$$

$$16\pi^2\beta_{y_t} = \frac{9}{2}y_t^3 - 8g_3^2y_t - \frac{9}{4}g_2^2y_t - \frac{17}{12}g_1^2y_t, \tag{A.4}$$

$$16\pi^2\beta_{\lambda} = 24\lambda^2 + \frac{\lambda_{hs}^2}{2} - 6y_t^4 + 12y_t^2\lambda - 9\lambda g_2^2 - 3\lambda g_1^2 + \frac{3}{8}g_1^4 + \frac{3}{4}g_2^2g_1^2 + \frac{9}{8}g_2^4, \tag{A.5}$$

$$16\pi^2\beta_{\lambda_{hs}} = 4\lambda_{hs}^2 + 6\lambda_s\lambda_{hs} - \frac{9}{2}\lambda_{hs}g_2^2 - \frac{3}{2}\lambda_{hs}g_1^2 + 6\lambda_{hs}y_t^2 + 12\lambda_{hs}\lambda, \tag{A.6}$$

$$16\pi^2\beta_{\lambda_s} = 2\lambda_{hs} + 18\lambda_s^2, \tag{A.7}$$

with

$$\beta_g = \frac{dg}{dt}, \quad t = \log\mu, \tag{A.8}$$

where g_1, g_2, g_3 are the $\mathrm{U}(1)_Y$, $\mathrm{SU}(2)_L$ and $\mathrm{SU}(3)_c$ gauge couplings. Following [176] we impose as initial conditions

$$g_1(M_Z) = 0.344, \tag{A.9}$$

$$g_2(M_Z) = 0.64, \tag{A.10}$$

$$g_3(M_Z) = 1.22. \tag{A.11}$$

JHEP01(2023)093

We solve the RGE evolution equations from the electroweak scale $\mu = 246\,\text{GeV}$ up to a maximum scale $\mu = \Lambda_{\text{max}}$ at which the quartic couplings fulfill the positivity and perturbativity conditions. We consider the point to be ruled out if $\Lambda_{\text{max}} < \Lambda_{\text{CP}}$.

References

[1] V.A. Kuzmin, V.A. Rubakov and M.E. Shaposhnikov, *On the Anomalous Electroweak Baryon Number Nonconservation in the Early Universe*, *Phys. Lett. B* **155** (1985) 36 [INSPIRE].

[2] A.G. Cohen, D.B. Kaplan and A.E. Nelson, *Progress in electroweak baryogenesis*, *Ann. Rev. Nucl. Part. Sci.* **43** (1993) 27 [hep-ph/9302210] [INSPIRE].

[3] V.A. Rubakov and M.E. Shaposhnikov, *Electroweak baryon number nonconservation in the early universe and in high-energy collisions*, *Usp. Fiz. Nauk* **166** (1996) 493 [hep-ph/9603208] [INSPIRE].

[4] D.E. Morrissey and M.J. Ramsey-Musolf, *Electroweak baryogenesis*, *New J. Phys.* **14** (2012) 125003 [arXiv:1206.2942] [INSPIRE].

[5] K. Kajantie, M. Laine, K. Rummukainen and M.E. Shaposhnikov, *Is there a hot electroweak phase transition at $m_H \gtrsim m_W$?*, *Phys. Rev. Lett.* **77** (1996) 2887 [hep-ph/9605288] [INSPIRE].

[6] C. Caprini et al., *Science with the space-based interferometer eLISA. II: Gravitational waves from cosmological phase transitions*, *JCAP* **04** (2016) 001 [arXiv:1512.06239] [INSPIRE].

[7] C. Caprini et al., *Detecting gravitational waves from cosmological phase transitions with LISA: an update*, *JCAP* **03** (2020) 024 [arXiv:1910.13125] [INSPIRE].

[8] AEDGE collaboration, *AEDGE: Atomic Experiment for Dark Matter and Gravity Exploration in Space*, *EPJ Quant. Technol.* **7** (2020) 6 [arXiv:1908.00802] [INSPIRE].

[9] L. Badurina, O. Buchmueller, J. Ellis, M. Lewicki, C. McCabe and V. Vaskonen, *Prospective sensitivities of atom interferometers to gravitational waves and ultralight dark matter*, *Phil. Trans. A. Math. Phys. Eng. Sci.* **380** (2021) 20210060 [arXiv:2108.02468] [INSPIRE].

[10] G.C. Dorsch, S.J. Huber and J.M. No, *Cosmological Signatures of a UV-Conformal Standard Model*, *Phys. Rev. Lett.* **113** (2014) 121801 [arXiv:1403.5583] [INSPIRE].

[11] J. Jaeckel, V.V. Khoze and M. Spannowsky, *Hearing the signal of dark sectors with gravitational wave detectors*, *Phys. Rev. D* **94** (2016) 103519 [arXiv:1602.03901] [INSPIRE].

[12] R. Jinno and M. Takimoto, *Probing a classically conformal B-L model with gravitational waves*, *Phys. Rev. D* **95** (2017) 015020 [arXiv:1604.05035] [INSPIRE].

[13] M. Chala, G. Nardini and I. Sobolev, *Unified explanation for dark matter and electroweak baryogenesis with direct detection and gravitational wave signatures*, *Phys. Rev. D* **94** (2016) 055006 [arXiv:1605.08663] [INSPIRE].

[14] M. Chala, M. Ramos and M. Spannowsky, *Gravitational wave and collider probes of a triplet Higgs sector with a low cutoff*, *Eur. Phys. J. C* **79** (2019) 156 [arXiv:1812.01901] [INSPIRE].

JHEP01(2023)093

[15] M. Artymowski, M. Lewicki and J.D. Wells, *Gravitational wave and collider implications of electroweak baryogenesis aided by non-standard cosmology*, *JHEP* **03** (2017) 066 [arXiv:1609.07143] [INSPIRE].

[16] K. Hashino, M. Kakizaki, S. Kanemura, P. Ko and T. Matsui, *Gravitational waves and Higgs boson couplings for exploring first order phase transition in the model with a singlet scalar field*, *Phys. Lett. B* **766** (2017) 49 [arXiv:1609.00297] [INSPIRE].

[17] V. Vaskonen, *Electroweak baryogenesis and gravitational waves from a real scalar singlet*, *Phys. Rev. D* **95** (2017) 123515 [arXiv:1611.02073] [INSPIRE].

[18] G.C. Dorsch, S.J. Huber, T. Konstandin and J.M. No, *A Second Higgs Doublet in the Early Universe: Baryogenesis and Gravitational Waves*, *JCAP* **05** (2017) 052 [arXiv:1611.05874] [INSPIRE].

[19] A. Beniwal, M. Lewicki, J.D. Wells, M. White and A.G. Williams, *Gravitational wave, collider and dark matter signals from a scalar singlet electroweak baryogenesis*, *JHEP* **08** (2017) 108 [arXiv:1702.06124] [INSPIRE].

[20] I. Baldes, *Gravitational waves from the asymmetric-dark-matter generating phase transition*, *JCAP* **05** (2017) 028 [arXiv:1702.02117] [INSPIRE].

[21] L. Marzola, A. Racioppi and V. Vaskonen, *Phase transition and gravitational wave phenomenology of scalar conformal extensions of the Standard Model*, *Eur. Phys. J. C* **77** (2017) 484 [arXiv:1704.01034] [INSPIRE].

[22] Z. Kang, P. Ko and T. Matsui, *Strong first order EWPT & strong gravitational waves in Z_3-symmetric singlet scalar extension*, *JHEP* **02** (2018) 115 [arXiv:1706.09721] [INSPIRE].

[23] S. Iso, P.D. Serpico and K. Shimada, *QCD-Electroweak First-Order Phase Transition in a Supercooled Universe*, *Phys. Rev. Lett.* **119** (2017) 141301 [arXiv:1704.04955] [INSPIRE].

[24] M. Chala, C. Krause and G. Nardini, *Signals of the electroweak phase transition at colliders and gravitational wave observatories*, *JHEP* **07** (2018) 062 [arXiv:1802.02168] [INSPIRE].

[25] S. Bruggisser, B. Von Harling, O. Matsedonskyi and G. Servant, *Electroweak Phase Transition and Baryogenesis in Composite Higgs Models*, *JHEP* **12** (2018) 099 [arXiv:1804.07314] [INSPIRE].

[26] E. Megías, G. Nardini and M. Quirós, *Cosmological Phase Transitions in Warped Space: Gravitational Waves and Collider Signatures*, *JHEP* **09** (2018) 095 [arXiv:1806.04877] [INSPIRE].

[27] D. Croon, V. Sanz and G. White, *Model Discrimination in Gravitational Wave spectra from Dark Phase Transitions*, *JHEP* **08** (2018) 203 [arXiv:1806.02332] [INSPIRE].

[28] A. Alves, T. Ghosh, H.-K. Guo, K. Sinha and D. Vagie, *Collider and Gravitational Wave Complementarity in Exploring the Singlet Extension of the Standard Model*, *JHEP* **04** (2019) 052 [arXiv:1812.09333] [INSPIRE].

[29] P. Baratella, A. Pomarol and F. Rompineve, *The Supercooled Universe*, *JHEP* **03** (2019) 100 [arXiv:1812.06996] [INSPIRE].

[30] A. Angelescu and P. Huang, *Multistep Strongly First Order Phase Transitions from New Fermions at the TeV Scale*, *Phys. Rev. D* **99** (2019) 055023 [arXiv:1812.08293] [INSPIRE].

[31] D. Croon, T.E. Gonzalo and G. White, *Gravitational Waves from a Pati-Salam Phase Transition*, *JHEP* **02** (2019) 083 [arXiv:1812.02747] [INSPIRE].

JHEP01(2023)093

[32] V. Brdar, A.J. Helmboldt and J. Kubo, *Gravitational Waves from First-Order Phase Transitions: LIGO as a Window to Unexplored Seesaw Scales*, *JCAP* **02** (2019) 021 [arXiv:1810.12306] [INSPIRE].

[33] A. Beniwal, M. Lewicki, M. White and A.G. Williams, *Gravitational waves and electroweak baryogenesis in a global study of the extended scalar singlet model*, *JHEP* **02** (2019) 183 [arXiv:1810.02380] [INSPIRE].

[34] M. Breitbach, J. Kopp, E. Madge, T. Opferkuch and P. Schwaller, *Dark, Cold, and Noisy: Constraining Secluded Hidden Sectors with Gravitational Waves*, *JCAP* **07** (2019) 007 [arXiv:1811.11175] [INSPIRE].

[35] C. Marzo, L. Marzola and V. Vaskonen, *Phase transition and vacuum stability in the classically conformal B-L model*, *Eur. Phys. J. C* **79** (2019) 601 [arXiv:1811.11169] [INSPIRE].

[36] I. Baldes and C. Garcia-Cely, *Strong gravitational radiation from a simple dark matter model*, *JHEP* **05** (2019) 190 [arXiv:1809.01198] [INSPIRE].

[37] T. Prokopec, J. Rezacek and B. Świeżewska, *Gravitational waves from conformal symmetry breaking*, *JCAP* **02** (2019) 009 [arXiv:1809.11129] [INSPIRE].

[38] M. Fairbairn, E. Hardy and A. Wickens, *Hearing without seeing: gravitational waves from hot and cold hidden sectors*, *JHEP* **07** (2019) 044 [arXiv:1901.11038] [INSPIRE].

[39] A.J. Helmboldt, J. Kubo and S. van der Woude, *Observational prospects for gravitational waves from hidden or dark chiral phase transitions*, *Phys. Rev. D* **100** (2019) 055025 [arXiv:1904.07891] [INSPIRE].

[40] P.S.B. Dev, F. Ferrer, Y. Zhang and Y. Zhang, *Gravitational Waves from First-Order Phase Transition in a Simple Axion-Like Particle Model*, *JCAP* **11** (2019) 006 [arXiv:1905.00891] [INSPIRE].

[41] S.A.R. Ellis, S. Ipek and G. White, *Electroweak Baryogenesis from Temperature-Varying Couplings*, *JHEP* **08** (2019) 002 [arXiv:1905.11994] [INSPIRE].

[42] R. Jinno, T. Konstandin and M. Takimoto, *Relativistic bubble collisions — a closer look*, *JCAP* **09** (2019) 035 [arXiv:1906.02588] [INSPIRE].

[43] J. Ellis, M. Fairbairn, M. Lewicki, V. Vaskonen and A. Wickens, *Intergalactic Magnetic Fields from First-Order Phase Transitions*, *JCAP* **09** (2019) 019 [arXiv:1907.04315] [INSPIRE].

[44] A. Azatov, D. Barducci and F. Sgarlata, *Gravitational traces of broken gauge symmetries*, *JCAP* **07** (2020) 027 [arXiv:1910.01124] [INSPIRE].

[45] B. Von Harling, A. Pomarol, O. Pujolàs and F. Rompineve, *Peccei-Quinn Phase Transition at LIGO*, *JHEP* **04** (2020) 195 [arXiv:1912.07587] [INSPIRE].

[46] L. Delle Rose, G. Panico, M. Redi and A. Tesi, *Gravitational Waves from Supercool Axions*, *JHEP* **04** (2020) 025 [arXiv:1912.06139] [INSPIRE].

[47] M. Barroso Mancha, T. Prokopec and B. Świeżewska, *Field-theoretic derivation of bubble-wall force*, *JHEP* **01** (2021) 070 [arXiv:2005.10875] [INSPIRE].

[48] A. Azatov and M. Vanvlasselaer, *Bubble wall velocity: heavy physics effects*, *JCAP* **01** (2021) 058 [arXiv:2010.02590] [INSPIRE].

[49] F. Giese, T. Konstandin, K. Schmitz and J. van de Vis, *Model-independent energy budget for LISA*, *JCAP* **01** (2021) 072 [arXiv:2010.09744] [INSPIRE].

JHEP01(2023)093

[50] I. Baldes, Y. Gouttenoire and F. Sala, *String Fragmentation in Supercooled Confinement and Implications for Dark Matter*, *JHEP* **04** (2021) 278 [arXiv:2007.08440] [INSPIRE].

[51] S. Höche, J. Kozaczuk, A.J. Long, J. Turner and Y. Wang, *Towards an all-orders calculation of the electroweak bubble wall velocity*, *JCAP* **03** (2021) 009 [arXiv:2007.10343] [INSPIRE].

[52] D. Croon, O. Gould, P. Schicho, T.V.I. Tenkanen and G. White, *Theoretical uncertainties for cosmological first-order phase transitions*, *JHEP* **04** (2021) 055 [arXiv:2009.10080] [INSPIRE].

[53] F.R. Ares, M. Hindmarsh, C. Hoyos and N. Jokela, *Gravitational waves from a holographic phase transition*, *JHEP* **21** (2020) 100 [arXiv:2011.12878] [INSPIRE].

[54] R.-G. Cai and S.-J. Wang, *Effective picture of bubble expansion*, *JCAP* **03** (2021) 096 [arXiv:2011.11451] [INSPIRE].

[55] F. Bigazzi, A. Caddeo, A.L. Cotrone and A. Paredes, *Dark Holograms and Gravitational Waves*, *JHEP* **04** (2021) 094 [arXiv:2011.08757] [INSPIRE].

[56] X. Wang, F.P. Huang and X. Zhang, *Bubble wall velocity beyond leading-log approximation in electroweak phase transition*, arXiv:2011.12903 [INSPIRE].

[57] I. Baldes, Y. Gouttenoire, F. Sala and G. Servant, *Supercool composite Dark Matter beyond* 100 *TeV*, *JHEP* **07** (2022) 084 [arXiv:2110.13926] [INSPIRE].

[58] Y. Gouttenoire, R. Jinno and F. Sala, *Friction pressure on relativistic bubble walls*, *JHEP* **05** (2022) 004 [arXiv:2112.07686] [INSPIRE].

[59] H. Yang, F.F. Freitas, A. Marciano, A.P. Morais, R. Pasechnik and J. Viana, *Gravitational-wave signatures of chiral-symmetric technicolor*, *Phys. Lett. B* **830** (2022) 137162 [arXiv:2204.00799] [INSPIRE].

[60] R. Zhou, L. Bian and Y. Du, *Electroweak phase transition and gravitational waves in the type-II seesaw model*, *JHEP* **08** (2022) 205 [arXiv:2203.01561] [INSPIRE].

[61] D. Brzeminski, A. Hook and G. Marques-Tavares, *Precision early universe cosmology from stochastic gravitational waves*, *JHEP* **11** (2022) 061 [arXiv:2203.13842] [INSPIRE].

[62] A. Azatov, G. Barni, S. Chakraborty, M. Vanvlasselaer and W. Yin, *Ultra-relativistic bubbles from the simplest Higgs portal and their cosmological consequences*, *JHEP* **10** (2022) 017 [arXiv:2207.02230] [INSPIRE].

[63] J.R. Espinosa and M. Quirós, *The Electroweak phase transition with a singlet*, *Phys. Lett. B* **305** (1993) 98 [hep-ph/9301285] [INSPIRE].

[64] S. Profumo, M.J. Ramsey-Musolf and G. Shaughnessy, *Singlet Higgs phenomenology and the electroweak phase transition*, *JHEP* **08** (2007) 010 [arXiv:0705.2425] [INSPIRE].

[65] J.R. Espinosa, T. Konstandin and F. Riva, *Strong Electroweak Phase Transitions in the Standard Model with a Singlet*, *Nucl. Phys. B* **854** (2012) 592 [arXiv:1107.5441] [INSPIRE].

[66] A. Noble and M. Perelstein, *Higgs self-coupling as a probe of electroweak phase transition*, *Phys. Rev. D* **78** (2008) 063518 [arXiv:0711.3018] [INSPIRE].

[67] J.M. No and M. Ramsey-Musolf, *Probing the Higgs Portal at the LHC Through Resonant di-Higgs Production*, *Phys. Rev. D* **89** (2014) 095031 [arXiv:1310.6035] [INSPIRE].

[68] D. Curtin, P. Meade and C.-T. Yu, *Testing Electroweak Baryogenesis with Future Colliders*, *JHEP* **11** (2014) 127 [arXiv:1409.0005] [INSPIRE].

JHEP01(2023)093

[69] T. Huang et al., *Resonant di-Higgs boson production in the $b\bar{b}WW$ channel: Probing the electroweak phase transition at the LHC*, *Phys. Rev. D* **96** (2017) 035007 [arXiv:1701.04442] [INSPIRE].

[70] S. Balaji, P.S.B. Dev, J. Silk and Y. Zhang, *Improved stellar limits on a light CP-even scalar*, *JCAP* **12** (2022) 024 [arXiv:2205.01669] [INSPIRE].

[71] M. Ibe, S. Kobayashi, Y. Nakayama and S. Shirai, *Cosmological constraints on dark scalar*, *JHEP* **03** (2022) 198 [arXiv:2112.11096] [INSPIRE].

[72] V. Barger, P. Langacker, M. McCaskey, M.J. Ramsey-Musolf and G. Shaughnessy, *LHC Phenomenology of an Extended Standard Model with a Real Scalar Singlet*, *Phys. Rev. D* **77** (2008) 035005 [arXiv:0706.4311] [INSPIRE].

[73] X.-G. He, T. Li, X.-Q. Li, J. Tandean and H.-C. Tsai, *The Simplest Dark-Matter Model, CDMS II Results, and Higgs Detection at LHC*, *Phys. Lett. B* **688** (2010) 332 [arXiv:0912.4722] [INSPIRE].

[74] M. Gonderinger, Y. Li, H. Patel and M.J. Ramsey-Musolf, *Vacuum Stability, Perturbativity, and Scalar Singlet Dark Matter*, *JHEP* **01** (2010) 053 [arXiv:0910.3167] [INSPIRE].

[75] J.M. Cline, K. Kainulainen, P. Scott and C. Weniger, *Update on scalar singlet dark matter*, *Phys. Rev. D* **88** (2013) 055025 [arXiv:1306.4710] [*Erratum ibid.* **92** (2015) 039906] [INSPIRE].

[76] D. Croon and G. White, *Exotic Gravitational Wave Signatures from Simultaneous Phase Transitions*, *JHEP* **05** (2018) 210 [arXiv:1803.05438] [INSPIRE].

[77] J.R. Espinosa, B. Gripaios, T. Konstandin and F. Riva, *Electroweak Baryogenesis in Non-minimal Composite Higgs Models*, *JCAP* **01** (2012) 012 [arXiv:1110.2876] [INSPIRE].

[78] J.M. Cline and K. Kainulainen, *Electroweak baryogenesis and dark matter from a singlet Higgs*, *JCAP* **01** (2013) 012 [arXiv:1210.4196] [INSPIRE].

[79] A. Alves, T. Ghosh, H.-K. Guo and K. Sinha, *Resonant Di-Higgs Production at Gravitational Wave Benchmarks: A Collider Study using Machine Learning*, *JHEP* **12** (2018) 070 [arXiv:1808.08974] [INSPIRE].

[80] A. Alves, D. Gonçalves, T. Ghosh, H.-K. Guo and K. Sinha, *Di-Higgs Production in the 4b Channel and Gravitational Wave Complementarity*, *JHEP* **03** (2020) 053 [arXiv:1909.05268] [INSPIRE].

[81] A. Alves, D. Gonçalves, T. Ghosh, H.-K. Guo and K. Sinha, *Di-Higgs Blind Spots in Gravitational Wave Signals*, *Phys. Lett. B* **818** (2021) 136377 [arXiv:2007.15654] [INSPIRE].

[82] S. Blasi and A. Mariotti, *Domain Walls Seeding the Electroweak Phase Transition*, *Phys. Rev. Lett.* **129** (2022) 261303 [arXiv:2203.16450] [INSPIRE].

[83] J.M. Cline and K. Kainulainen, *A New source for electroweak baryogenesis in the MSSM*, *Phys. Rev. Lett.* **85** (2000) 5519 [hep-ph/0002272] [INSPIRE].

[84] M. Joyce, T. Prokopec and N. Turok, *Nonlocal electroweak baryogenesis. Part 2: The Classical regime*, *Phys. Rev. D* **53** (1996) 2958 [hep-ph/9410282] [INSPIRE].

[85] M. Joyce, T. Prokopec and N. Turok, *Electroweak baryogenesis from a classical force*, *Phys. Rev. Lett.* **75** (1995) 1695 [hep-ph/9408339] [*Erratum ibid.* **75** (1995) 3375] [INSPIRE].

[86] A. Riotto, *Towards a nonequilibrium quantum field theory approach to electroweak baryogenesis*, *Phys. Rev. D* **53** (1996) 5834 [hep-ph/9510271] [INSPIRE].

JHEP01(2023)093

[87] A. Riotto, *Supersymmetric electroweak baryogenesis, nonequilibrium field theory and quantum Boltzmann equations*, *Nucl. Phys. B* **518** (1998) 339 [hep-ph/9712221] [INSPIRE].

[88] K. Kainulainen, *CP-violating transport theory for electroweak baryogenesis with thermal corrections*, *JCAP* **11** (2021) 042 [arXiv:2108.08336] [INSPIRE].

[89] M. Postma, J. van de Vis and G. White, *Resummation and cancellation of the VIA source in electroweak baryogenesis*, *JHEP* **12** (2022) 121 [arXiv:2206.01120] [INSPIRE].

[90] J.M. Cline and B. Laurent, *Electroweak baryogenesis from light fermion sources: A critical study*, *Phys. Rev. D* **104** (2021) 083507 [arXiv:2108.04249] [INSPIRE].

[91] J.M. Cline and K. Kainulainen, *Electroweak baryogenesis at high bubble wall velocities*, *Phys. Rev. D* **101** (2020) 063525 [arXiv:2001.00568] [INSPIRE].

[92] B. Laurent and J.M. Cline, *Fluid equations for fast-moving electroweak bubble walls*, *Phys. Rev. D* **102** (2020) 063516 [arXiv:2007.10935] [INSPIRE].

[93] J.M. Cline, A. Friedlander, D.-M. He, K. Kainulainen, B. Laurent and D. Tucker-Smith, *Baryogenesis and gravity waves from a UV-completed electroweak phase transition*, *Phys. Rev. D* **103** (2021) 123529 [arXiv:2102.12490] [INSPIRE].

[94] M. Lewicki, M. Merchand and M. Zych, *Electroweak bubble wall expansion: gravitational waves and baryogenesis in Standard Model-like thermal plasma*, *JHEP* **02** (2022) 017 [arXiv:2111.02393] [INSPIRE].

[95] E.J. Weinberg, *Radiative corrections as the origin of spontaneous symmetry breaking*, Ph.D. Thesis, Harvard University (1973) [hep-th/0507214] [INSPIRE].

[96] S. Weinberg, *Gauge and Global Symmetries at High Temperature*, *Phys. Rev. D* **9** (1974) 3357 [INSPIRE].

[97] L. Niemi, P. Schicho and T.V.I. Tenkanen, *Singlet-assisted electroweak phase transition at two loops*, *Phys. Rev. D* **103** (2021) 115035 [arXiv:2103.07467] [INSPIRE].

[98] P.M. Schicho, T.V.I. Tenkanen and J. Österman, *Robust approach to thermal resummation: Standard Model meets a singlet*, *JHEP* **06** (2021) 130 [arXiv:2102.11145] [INSPIRE].

[99] P. Schicho, T.V.I. Tenkanen and G. White, *Combining thermal resummation and gauge invariance for electroweak phase transition*, *JHEP* **11** (2022) 047 [arXiv:2203.04284] [INSPIRE].

[100] A. Ekstedt, P. Schicho and T.V.I. Tenkanen, *DRalgo: a package for effective field theory approach for thermal phase transitions*, HIP-2022-11/TH (2022) [INSPIRE].

[101] C.L. Wainwright, *CosmoTransitions: Computing Cosmological Phase Transition Temperatures and Bubble Profiles with Multiple Fields*, *Comput. Phys. Commun.* **183** (2012) 2006 [arXiv:1109.4189] [INSPIRE].

[102] K. Saikawa and S. Shirai, *Primordial gravitational waves, precisely: The role of thermodynamics in the Standard Model*, *JCAP* **05** (2018) 035 [arXiv:1803.01038] [INSPIRE].

[103] J. Ellis, M. Lewicki and J.M. No, *On the Maximal Strength of a First-Order Electroweak Phase Transition and its Gravitational Wave Signal*, *JCAP* **04** (2019) 003 [arXiv:1809.08242] [INSPIRE].

[104] M. Carena, Z. Liu and Y. Wang, *Electroweak phase transition with spontaneous Z_2-breaking*, *JHEP* **08** (2020) 107 [arXiv:1911.10206] [INSPIRE].

JHEP01(2023)093

[105] F. Bigazzi, A. Caddeo, T. Canneti and A.L. Cotrone, *Bubble wall velocity at strong coupling*, *JHEP* **08** (2021) 090 [arXiv:2104.12817] [INSPIRE].

[106] Y. Bea, J. Casalderrey-Solana, T. Giannakopoulos, D. Mateos, M. Sanchez-Garitaonandia and M. Zilhão, *Bubble wall velocity from holography*, *Phys. Rev. D* **104** (2021) L121903 [arXiv:2104.05708] [INSPIRE].

[107] T. Konstandin and J.M. No, *Hydrodynamic obstruction to bubble expansion*, *JCAP* **02** (2011) 008 [arXiv:1011.3735] [INSPIRE].

[108] S. Balaji, M. Spannowsky and C. Tamarit, *Cosmological bubble friction in local equilibrium*, *JCAP* **03** (2021) 051 [arXiv:2010.08013] [INSPIRE].

[109] W.-Y. Ai, B. Garbrecht and C. Tamarit, *Bubble wall velocities in local equilibrium*, *JCAP* **03** (2022) 015 [arXiv:2109.13710] [INSPIRE].

[110] S.-J. Wang and Z.-Y. Yuwen, *Hydrodynamic backreaction force of cosmological bubble expansion*, *Phys. Rev. D* **107** (2023) 023501 [arXiv:2205.02492] [INSPIRE].

[111] M. Dine, R.G. Leigh, P.Y. Huet, A.D. Linde and D.A. Linde, *Towards the theory of the electroweak phase transition*, *Phys. Rev. D* **46** (1992) 550 [hep-ph/9203203] [INSPIRE].

[112] B.-H. Liu, L.D. McLerran and N. Turok, *Bubble nucleation and growth at a baryon number producing electroweak phase transition*, *Phys. Rev. D* **46** (1992) 2668 [INSPIRE].

[113] D. Bodeker and G.D. Moore, *Can electroweak bubble walls run away?*, *JCAP* **05** (2009) 009 [arXiv:0903.4099] [INSPIRE].

[114] D. Bodeker and G.D. Moore, *Electroweak Bubble Wall Speed Limit*, *JCAP* **05** (2017) 025 [arXiv:1703.08215] [INSPIRE].

[115] B. Laurent and J.M. Cline, *First principles determination of bubble wall velocity*, *Phys. Rev. D* **106** (2022) 023501 [arXiv:2204.13120] [INSPIRE].

[116] G.C. Dorsch, S.J. Huber and T. Konstandin, *A sonic boom in bubble wall friction*, *JCAP* **04** (2022) 010 [arXiv:2112.12548] [INSPIRE].

[117] S. De Curtis, L.D. Rose, A. Guiggiani, A.G. Muyor and G. Panico, *Bubble wall dynamics at the electroweak phase transition*, *JHEP* **03** (2022) 163 [arXiv:2201.08220] [INSPIRE].

[118] G.D. Moore and T. Prokopec, *How fast can the wall move? A Study of the electroweak phase transition dynamics*, *Phys. Rev. D* **52** (1995) 7182 [hep-ph/9506475] [INSPIRE].

[119] G.D. Moore and T. Prokopec, *Bubble wall velocity in a first order electroweak phase transition*, *Phys. Rev. Lett.* **75** (1995) 777 [hep-ph/9503296] [INSPIRE].

[120] A. Friedlander, I. Banta, J.M. Cline and D. Tucker-Smith, *Wall speed and shape in singlet-assisted strong electroweak phase transitions*, *Phys. Rev. D* **103** (2021) 055020 [arXiv:2009.14295] [INSPIRE].

[121] J. Kozaczuk, *Bubble Expansion and the Viability of Singlet-Driven Electroweak Baryogenesis*, *JHEP* **10** (2015) 135 [arXiv:1506.04741] [INSPIRE].

[122] T. Konstandin, G. Nardini and I. Rues, *From Boltzmann equations to steady wall velocities*, *JCAP* **09** (2014) 028 [arXiv:1407.3132] [INSPIRE].

[123] S.J. Huber and M. Sopena, *An efficient approach to electroweak bubble velocities*, arXiv:1302.1044 [INSPIRE].

[124] P.J. Steinhardt, *Relativistic Detonation Waves and Bubble Growth in False Vacuum Decay*, *Phys. Rev. D* **25** (1982) 2074 [INSPIRE].

JHEP01(2023)093

[125] M. Kamionkowski, A. Kosowsky and M.S. Turner, *Gravitational radiation from first order phase transitions*, *Phys. Rev. D* **49** (1994) 2837 [astro-ph/9310044] [INSPIRE].

[126] J.R. Espinosa, T. Konstandin, J.M. No and G. Servant, *Energy Budget of Cosmological First-order Phase Transitions*, *JCAP* **06** (2010) 028 [arXiv:1004.4187] [INSPIRE].

[127] F. Pedregosa et al., *Scikit-learn: Machine Learning in Python*, *J. Mach. Learn. Res.* **12** (2011) 2825 [arXiv:1201.0490] [INSPIRE].

[128] J. Ellis, M. Lewicki, J.M. No and V. Vaskonen, *Gravitational wave energy budget in strongly supercooled phase transitions*, *JCAP* **06** (2019) 024 [arXiv:1903.09642] [INSPIRE].

[129] M. Lewicki and V. Vaskonen, *On bubble collisions in strongly supercooled phase transitions*, *Phys. Dark Univ.* **30** (2020) 100672 [arXiv:1912.00997] [INSPIRE].

[130] M. Lewicki and V. Vaskonen, *Gravitational wave spectra from strongly supercooled phase transitions*, *Eur. Phys. J. C* **80** (2020) 1003 [arXiv:2007.04967] [INSPIRE].

[131] M. Lewicki and V. Vaskonen, *Gravitational waves from colliding vacuum bubbles in gauge theories*, *Eur. Phys. J. C* **81** (2021) 437 [arXiv:2012.07826] [*Erratum ibid.* **81** (2021) 1077] [INSPIRE].

[132] M. Lewicki and V. Vaskonen, *Gravitational waves from bubble collisions and fluid motion in strongly supercooled phase transitions*, arXiv:2208.11697 [INSPIRE].

[133] A. Roper Pol, S. Mandal, A. Brandenburg, T. Kahniashvili and A. Kosowsky, *Numerical simulations of gravitational waves from early-universe turbulence*, *Phys. Rev. D* **102** (2020) 083512 [arXiv:1903.08585] [INSPIRE].

[134] T. Kahniashvili, A. Brandenburg, G. Gogoberidze, S. Mandal and A. Roper Pol, *Circular polarization of gravitational waves from early-Universe helical turbulence*, *Phys. Rev. Res.* **3** (2021) 013193 [arXiv:2011.05556] [INSPIRE].

[135] A. Roper Pol, S. Mandal, A. Brandenburg and T. Kahniashvili, *Polarization of gravitational waves from helical MHD turbulent sources*, *JCAP* **04** (2022) 019 [arXiv:2107.05356] [INSPIRE].

[136] P. Auclair et al., *Generation of gravitational waves from freely decaying turbulence*, *JCAP* **09** (2022) 029 [arXiv:2205.02588] [INSPIRE].

[137] M. Hindmarsh, S.J. Huber, K. Rummukainen and D.J. Weir, *Gravitational waves from the sound of a first order phase transition*, *Phys. Rev. Lett.* **112** (2014) 041301 [arXiv:1304.2433] [INSPIRE].

[138] M. Hindmarsh, S.J. Huber, K. Rummukainen and D.J. Weir, *Numerical simulations of acoustically generated gravitational waves at a first order phase transition*, *Phys. Rev. D* **92** (2015) 123009 [arXiv:1504.03291] [INSPIRE].

[139] M. Hindmarsh, S.J. Huber, K. Rummukainen and D.J. Weir, *Shape of the acoustic gravitational wave power spectrum from a first order phase transition*, *Phys. Rev. D* **96** (2017) 103520 [arXiv:1704.05871] [*Erratum ibid.* **101** (2020) 089902] [INSPIRE].

[140] M.B. Hindmarsh, M. Lüben, J. Lumma and M. Pauly, *Phase transitions in the early universe*, *SciPost Phys. Lect. Notes* **24** (2021) 1 [arXiv:2008.09136] [INSPIRE].

[141] J. Ellis, M. Lewicki and J.M. No, *Gravitational waves from first-order cosmological phase transitions: lifetime of the sound wave source*, *JCAP* **07** (2020) 050 [arXiv:2003.07360] [INSPIRE].

JHEP01(2023)093

[142] H.-K. Guo, K. Sinha, D. Vagie and G. White, *Phase Transitions in an Expanding Universe: Stochastic Gravitational Waves in Standard and Non-Standard Histories*, *JCAP* **01** (2021) 001 [arXiv:2007.08537] [INSPIRE].

[143] E. Thrane and J.D. Romano, *Sensitivity curves for searches for gravitational-wave backgrounds*, *Phys. Rev. D* **88** (2013) 124032 [arXiv:1310.5300] [INSPIRE].

[144] LIGO Scientific collaboration, *Advanced LIGO*, *Class. Quant. Grav.* **32** (2015) 074001 [arXiv:1411.4547] [INSPIRE].

[145] LIGO Scientific and Virgo collaborations, *GW150914: Implications for the stochastic gravitational wave background from binary black holes*, *Phys. Rev. Lett.* **116** (2016) 131102 [arXiv:1602.03847] [INSPIRE].

[146] LIGO Scientific and Virgo collaborations, *Search for the isotropic stochastic background using data from Advanced LIGO's second observing run*, *Phys. Rev. D* **100** (2019) 061101 [arXiv:1903.02886] [INSPIRE].

[147] N. Bartolo et al., *Science with the space-based interferometer LISA. IV: Probing inflation with gravitational waves*, *JCAP* **12** (2016) 026 [arXiv:1610.06481] [INSPIRE].

[148] C. Caprini et al., *Reconstructing the spectral shape of a stochastic gravitational wave background with LISA*, *JCAP* **11** (2019) 017 [arXiv:1906.09244] [INSPIRE].

[149] M. Punturo et al., *The Einstein Telescope: A third-generation gravitational wave observatory*, *Class. Quant. Grav.* **27** (2010) 194002 [INSPIRE].

[150] S. Hild et al., *Sensitivity Studies for Third-Generation Gravitational Wave Observatories*, *Class. Quant. Grav.* **28** (2011) 094013 [arXiv:1012.0908] [INSPIRE].

[151] L. Badurina et al., *AION: An Atom Interferometer Observatory and Network*, *JCAP* **05** (2020) 011 [arXiv:1911.11755] [INSPIRE].

[152] M. Lewicki and V. Vaskonen, *Impact of LIGO-Virgo binaries on gravitational wave background searches*, arXiv:2111.05847 [INSPIRE].

[153] M. Hindmarsh, *Sound shell model for acoustic gravitational wave production at a first-order phase transition in the early Universe*, *Phys. Rev. Lett.* **120** (2018) 071301 [arXiv:1608.04735] [INSPIRE].

[154] M. Hindmarsh and M. Hijazi, *Gravitational waves from first order cosmological phase transitions in the Sound Shell Model*, *JCAP* **12** (2019) 062 [arXiv:1909.10040] [INSPIRE].

[155] R. Jinno, T. Konstandin and H. Rubira, *A hybrid simulation of gravitational wave production in first-order phase transitions*, *JCAP* **04** (2021) 014 [arXiv:2010.00971] [INSPIRE].

[156] C. Gowling and M. Hindmarsh, *Observational prospects for phase transitions at LISA: Fisher matrix analysis*, *JCAP* **10** (2021) 039 [arXiv:2106.05984] [INSPIRE].

[157] ATLAS, CDF, CMS and D0 collaborations, *First combination of Tevatron and LHC measurements of the top-quark mass*, ATLAS-CONF-2014-008 (2014) [INSPIRE].

[158] Particle Data Group collaboration, *Review of Particle Physics*, *PTEP* **2020** (2020) 083C01 [INSPIRE].

[159] ATLAS collaboration, *A detailed map of Higgs boson interactions by the ATLAS experiment ten years after the discovery*, *Nature* **607** (2022) 52 [arXiv:2207.00092] [*Erratum ibid.* **612** (2022) E24] [INSPIRE].

JHEP01(2023)093

[160] CMS collaboration, *A portrait of the Higgs boson by the CMS experiment ten years after the discovery*, *Nature* **607** (2022) 60 [arXiv:2207.00043] [INSPIRE].

[161] CMS collaboration, *Measurements of $t\bar{t}H$ Production and the CP Structure of the Yukawa Interaction between the Higgs Boson and Top Quark in the Diphoton Decay Channel*, *Phys. Rev. Lett.* **125** (2020) 061801 [arXiv:2003.10866] [INSPIRE].

[162] J. Haller, A. Hoecker, R. Kogler, K. Mönig, T. Peiffer and J. Stelzer, *Update of the global electroweak fit and constraints on two-Higgs-doublet models*, *Eur. Phys. J. C* **78** (2018) 675 [arXiv:1803.01853] [INSPIRE].

[163] E. Bagnaschi, J. Ellis, M. Madigan, K. Mimasu, V. Sanz and T. You, *SMEFT analysis of m_W*, *JHEP* **08** (2022) 308 [arXiv:2204.05260] [INSPIRE].

[164] T. Robens and T. Stefaniak, *Status of the Higgs Singlet Extension of the Standard Model after LHC Run 1*, *Eur. Phys. J. C* **75** (2015) 104 [arXiv:1501.02234] [INSPIRE].

[165] ATLAS collaboration, *Search for heavy resonances decaying into a pair of Z bosons in the $\ell^+\ell^-\ell'^+\ell'^-$ and $\ell^+\ell^-\nu\bar{\nu}$ final states using 139 fb^{-1} of proton-proton collisions at $\sqrt{s} = 13$ TeV with the ATLAS detector*, *Eur. Phys. J. C* **81** (2021) 332 [arXiv:2009.14791] [INSPIRE].

[166] CMS collaboration, *Search for a new scalar resonance decaying to a pair of Z bosons in proton-proton collisions at $\sqrt{s} = 13$ TeV*, *JHEP* **06** (2018) 127 [arXiv:1804.01939] [*Erratum ibid.* **03** (2019) 128] [INSPIRE].

[167] CMS collaboration, *Measurement of Higgs Boson Production and Properties in the WW Decay Channel with Leptonic Final States*, *JHEP* **01** (2014) 096 [arXiv:1312.1129] [INSPIRE].

[168] ATLAS collaboration, *Search for an additional, heavy Higgs boson in the $H \to ZZ$ decay channel at $\sqrt{s} = 8$ TeV in pp collision data with the ATLAS detector*, *Eur. Phys. J. C* **76** (2016) 45 [arXiv:1507.05930] [INSPIRE].

[169] S.M. Barr and A. Zee, *Electric Dipole Moment of the Electron and of the Neutron*, *Phys. Rev. Lett.* **65** (1990) 21 [*Erratum ibid.* **65** (1990) 2920] [INSPIRE].

[170] V. Keus, N. Koivunen and K. Tuominen, *Singlet scalar and 2HDM extensions of the Standard Model: CP-violation and constraints from $(g-2)_\mu$ and eEDM*, *JHEP* **09** (2018) 059 [arXiv:1712.09613] [INSPIRE].

[171] ACME collaboration, *Improved limit on the electric dipole moment of the electron*, *Nature* **562** (2018) 355 [INSPIRE].

[172] G.C. Dorsch, S.J. Huber and T. Konstandin, *On the wall velocity dependence of electroweak baryogenesis*, *JCAP* **08** (2021) 020 [arXiv:2106.06547] [INSPIRE].

[173] J.M. No, *Large Gravitational Wave Background Signals in Electroweak Baryogenesis Scenarios*, *Phys. Rev. D* **84** (2011) 124025 [arXiv:1103.2159] [INSPIRE].

[174] X. Wu et al., *The metastable $Q^3\Delta_2$ state of ThO: a new resource for the ACME electron EDM search*, *New J. Phys.* **22** (2020) 023013 [arXiv:1911.03015] [INSPIRE].

[175] P. Ghorbani, *Vacuum stability vs. positivity in real singlet scalar extension of the standard model*, *Nucl. Phys. B* **971** (2021) 115533 [arXiv:2104.09542] [INSPIRE].

[176] J.A. Casas, J.R. Espinosa, M. Quirós and A. Riotto, *The Lightest Higgs boson mass in the minimal supersymmetric standard model*, *Nucl. Phys. B* **436** (1995) 3 [hep-ph/9407389] [*Erratum ibid.* **439** (1995) 466] [INSPIRE].

JHEP01(2023)093